Inhibition of histone acetyltransferase GCN5 by a transcription factor FgPacC controls fungal adaption to host-derived iron stress

Qin Gu[1,*,†], Yujie Wang[1,†], Xiaozhen Zhao[1], Bingqin Yuan[1], Mengxuan Zhang[1], Zheng Tan[1], Xinyue Zhang[1], Yun Chen [iD][2], Huijun Wu[1], Yuming Luo[3], Nancy P. Keller[4], Xuewen Gao[1,*] and Zhonghua Ma [iD][2,*]

[1]Department of Plant Pathology, College of Plant Protection, Nanjing Agricultural University, Key Laboratory of Monitoring and Management of Crop Diseases and Pest Insects, Ministry of Education, Nanjing, China, [2]State Key Laboratory of Rice Biology, the Key Laboratory of Molecular Biology of Crop Pathogens and Insects, Institute of Biotechnology, Zhejiang University, Hangzhou, China, [3]Jiangsu Key Laboratory for Eco-Agricultural Biotechnology around Hongze Lake, Jiangsu Collaborative Innovation Center of Regional Modern Agriculture and Environmental Protection, Huaiyin Normal University, Huai'an, China and [4]Department of Medical Microbiology and Immunology, University of Wisconsin-Madison, Madison, WI, USA

ABSTRACT

Poaceae plants can locally accumulate iron to suppress pathogen infection. It remains unknown how pathogens overcome host-derived iron stress during their successful infections. Here, we report that *Fusarium graminearum* (Fg), a destructive fungal pathogen of cereal crops, is challenged by host-derived high-iron stress. Fg infection induces host alkalinization, and the pH-dependent transcription factor FgPacC undergoes a proteolytic cleavage into the functional isoform named FgPacC30 under alkaline host environment. Subsequently FgPacC30 binds to a GCCAR(R = A/G)G element at the promoters of the genes involved in iron uptake and inhibits their expression, leading to adaption of Fg to high-iron stress. Mechanistically, FgPacC30 binds to FgGcn5 protein, a catalytic subunit of Spt-Ada-Gcn5 Acetyltransferase (SAGA) complex, leading to deregulation of histone acetylation at H3K18 and H2BK11, and repression of iron uptake genes. Moreover, we identified a protein kinase FgHal4, which is highly induced by extracellular high-iron stress and protects FgPacC30 against 26S proteasome-dependent degradation by promoting FgPacC30 phosphorylation at Ser2. Collectively, this study uncovers a novel inhibitory mechanism of the SAGA complex by a transcription factor that enables a fungal pathogen to adapt to dynamic microenvironments during infection.

GRAPHICAL ABSTRACT
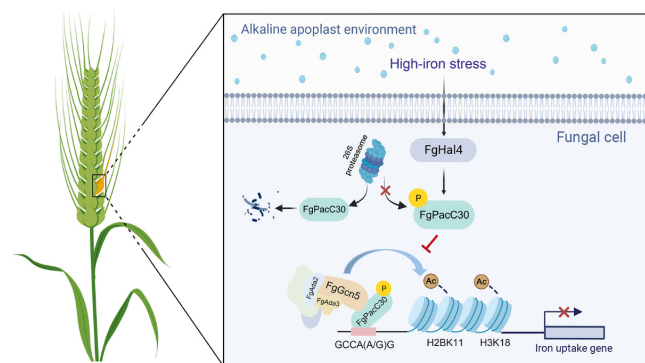
INTRODUCTION

The redox-active metal iron (Fe) is an essential cofactor for a variety of essential cellular processes, including DNA replication and energy production (1,2). Although iron scarcity is harmful for the survival and development of eukaryotes, iron overload leads to the generation of toxic ROS via Fenton reaction resulting in damages to various cellular components (3). Therefore, many eukaryotic organisms,

---

including plants and phytopathogens, have evolved sophisticated strategies to tightly regulate iron acquisition, consumption and storage, thus maintaining intracellular iron homeostasis.

Iron is a focus of the struggle in host–pathogen interactions (4,5). During mammalian-pathogen interactions, mammals use iron-withholding strategies to prevent pathogens from invading the host (4,6). In line with this, some host plants deploy similar mechanisms, such as synthesizing iron-sequestering ferritin and defensins, to interfere with pathogen scavenging for iron, and consequently reducing infections by pathogens (7–9). In contrast to withholding iron to reduce pathogen proliferation, some plants, particularly Poaceae, can locally accumulate iron to prevent pathogen infection (5,10,11). For example, wheat plants can locally increase iron levels and promote cereal defenses against *Blumeria graminis* infection (12). Similarly, maize with an adequate iron nutritional status may also recruit free iron to the infection site to suppress fungal infection of *Colletotrichum graminicola* (13). While it is known that local iron accumulation is a ubiquitous defense response in plants, it remains largely unknown how pathogens counteract host-derived high-iron stress.

Microbial pathogens encounter dynamic microenvironments during infection. Extensive transcription reprogramming enables microorganisms to precisely respond to changes of host environments (14,15). Histone acetylation that serves as as a switch between repressive and active chromatin status has been implicated as a fundamental mechanism of transcriptional regulation (16,17). Histone acetylation is tightly regulated by histone acetyltransferases (HATs) and histone deacetylases (HDACs), which can be recruited by specific transcriptional activators and repressors to its target genes. The evolutionary conserved Spt-ADA-Gcn5-Acetyltransferase (SAGA) complex consisting of the HAT Gcn5 and its interacting partner Ada2/Ada3 is a multi-module assembly that controls eukaryotic transcription by modifying histones (18,19). The human SAGA complex plays a genome-wide role in transcriptional activation and is required for RNA polymerase II transcription (20). In yeast, rapid depletion of SAGA complex leads to transcription defects of ∼13% protein-coding genes (21). In fungal pathogens, Gcn5-mediated histone acetylation is important for regulating the genes involved in host environment adaption and fungal virulence (15). For example, the ΔGcn5 mutant of *Candida albicans* exhibits hypersensitivity to host-derived oxidative stresses and attenuated virulence (22). Gcn5 is important in responding to the specific environmental conditions encountered by *Cryptococcus neoformans* within the host. Accordingly, the ΔGcn5 mutant is avirulent in animal models of cryptococcosis (23). Similarly, disruption of Gcn5 also results in attenuated virulence in plant fungal pathogens, such as *Fusarium graminearum*, *Ustilago maydis* and *Fusarium fujikuroi* (24–26), and is important for secondary metabolism and asexual spore production in *Aspergillus* spp. (27–28). Although it has been well known that the SAGA-mediated histone acetylation is critical for regulating gene transcription in response of fungi to host environmental cues, the underlying molecular mechanisms that regulate the assembly and activity of SAGA complex remain to be documented.

F. graminearum (named Fg thereafter) is an economically devastating fungal pathogen that causes cereal scab in the world (29,30). In recent years, wheat-Fg has emerged as an important pathosystem for investigating fungal pathogenesis. Here, we show that in wheat-Fg interactions, Fg is exposed to host-derived high-iron stress during infection. To overcome this stress, the pathogen is able to induce plant alkalinization, and the fungal transcription factor FgPacC undergoes a proteolytic cleavage into FgPacC30 during host pH upshifts, which directly binds to the promoters of Fg iron uptake genes and represses their expression. Mechanistically, we demonstrate that FgPacC30 binds and inhibits the activity of FgGcn5, a histone acetyltransferase of the SAGA complex. Subsequently, FgPacC30 deregulates H3K18 and H2BK11 acetylation and suppresses the expression of iron uptake genes. Additionally, we identified a protein kinase FgHal4 that is involved in the phosphorylation of FgPacC30 under high-iron conditions, and thereby protecting FgPacC30 against 26S proteasome-dependent degradation. Taken together, this study demonstrates that the transcription factor FgPacC plays a key role in protecting the fungus from iron toxicity through direct binding of promoters and inhibition of SAGA activity. This work illustrates adaptation of a fungal pathogen to host-derived iron stress at an epigenetic level, which provides a conceptual regulatory mechanism for understanding fungal adaption to a host-derived stress.

MATERIALS AND METHODS

Fungal Strains and growth determination

The Fg wild-type strain PH-1 (NRRL 31084) was used as a parental strain throughout this study (31). Mycelial growth of the wild-type PH-1 and its derivative strains were assayed on minimal medium (MM; 0.5 g KCl, 0.5 g $MgSO_4 \cdot 7H_2O$, 1 g KH_2PO_4, 2 g $NaNO_3$, 0.01 g $FeSO_4 \cdot 7H_2O$, 30 g sucrose, 200 μl of trace element solution (per 100 ml, 5 g citric acid, 5 g $ZnSO_4 \cdot 6H_2O$, 0.25 g $CuSO_4 \cdot 5H_2O$, 1 g $Fe(NH_4)_2(SO_4)_2 \cdot 6H_2O$, 10 g agar and 1 l water) adjusted to different pH with appropriate buffers, and further supplemented with or without 5 mM iron (Fe^{2+}). The mycelial radial growth (colony diameter) of each strain was measured with a calliper gauge along two diameters at right angles to one another, and the average diameter for each plate was calculated as described by Weitz *et al.* (32).

Mutant generation and complementation

Targeted gene replacement with hygromycin resistance cassette using polyethylene glycol (PEG) mediated protoplast transformation method was performed as reported previously (33). Primers used for gene replacement and identification of mutants are listed in Supplementary Table S1. The deletion mutants of *FgPACC* and *FgHAL4* were further confirmed by Southern blot assays (Supplementary Figure S1).

To complement the deletion mutants, the full-length *Fg-PACC* or *FgHAL4* fragment with its native promoter sequence was co-transformed with XhoI-digested pYF11 into the yeast strain XK1-25 by yeast gap repair approach (34).

The resulting pYF11:: *FgPACC* or pYF11::*FgHAL4* construct was transformed into the protoplast of ΔFgPacC or ΔFgHal4 mutant, respectively. The resulting geneticin-resistant transformants were confirmed by Southern blot assays (Supplementary Figure S1). All of the mutants generated in this study were preserved in 15% glycerol at −80°C.

Plant infection assays

The pathogenicity of each strain on flowering wheat (*Triticum aestivum*) head and seedling leaf was assessed as described previously (31,35). Briefly, a 10 μl aliquot of conidial suspension (10^5 conidia/ml) of each strain was injected in the palea in middle spikelet of a wheat head. The control wheat head was inoculated with a 10 μl aliquot of sterilized water. Spikelets with typical wheat scab symptoms were examined at 14 day post-inoculation (dpi) to calculate the disease index (36). The mean ± standard deviation of the disease index was calculated with data from three biological replicates with at least ten wheat heads examined in each replicate.

To assay Fg infection on wheat seedling leaf, a 5-mm mycelial plug collected from the edge of 3-day-old colony was inoculated on a 14-day-old seedling leaf, and the inoculated leaves were incubated at 25°C and 100% humidity with 12 h of daylight. Data were presented as the mean ± standard deviation three biological replicates with at least 10 seedling leaves examined in each replicate showing the lesion area by ImageJ.

Staining procedures and microscopy observation

For investigating plant alkalinization and iron accumulation in wheat plant in response to Fg attack, the wheat heads (palea tissues) or seedling leaves inoculated with Fg at 24, 48 and 120 h post-inoculation (hpi) were stained with 1 mM 8-hydroxypyrene-1,3,6-trisulfonic acid trisodium salt (HPTS) (H1529, Sigma-Aldrich, St. Louis, MO, USA) or 5 μM FeRhoNox™-1 (GC901, Goryo Chemical, Inc., Sapporo, Japan) in an incubator with 5% CO_2 for 60 min at 37°C, and then washed three times with sterile PBS as described previously (37,38). Fluorescent signals of the pH indicator HPTS in the protonated form (excitation 405 nm) and deprotonated form (excitation 458 nm) were detected under a Zeiss LSM710 microscope (Gottingen, Niedersachsen, Germany). The image analyses were performed using the Fiji software (https://fiji.sc/) with 'ratiometric' macro. Fluorescent signals of the Fe^{2+} indicator FeRhoNox™-1 were examined under a Nikon SMZ25 microscope with the excitation/emission wavelengths of 532 nm/570 nm.

Determination of iron and pH in apoplastic fluids of wheat plants

Extraction of apoplastic fluids was performed by using a previously described method with slight modifications (39). Briefly, 14-day-old wheat seedling leaves inoculated with Fg at different time intervals were washed and vacuum infiltrated with cold water twice for 2 min. Apoplastic fluids were collected by centrifugation at 3000 × *g* for 5 min, and then were used for further iron content and pH measurement.

Iron content of apoplastic fluids from Fg infected wheat seedling leaves were assayed by using an Iron Assay Kit (Abcam, ab83366), and Fe^{2+} content was measured by using the Synergy H1 microplate reader (OD = 593 nm; Biotek Instruments, Winooski, VT, USA) following the manufacturer's instructions (40). The pH of apoplastic fluids from wheat seedling leaves and palea tissues sampled at different time intervals after Fg inoculation was measured with a pH electrode (model PHM93, Radiometer Analytical).

RNA-seq analysis and RT-qPCR

For *in vitro* and *in planta* fungal transcriptome analysis, the wheat seedling leaves infected with Fg were sampled at 24, 48 and 120 h post-inoculation (hpi) for total RNA extraction using TRIZOL reagent (TaKaRa, Dalian, China) following the manufacturer's instructions. In addition, samples of mycelia used for inoculation were collected to represent the time point of 0 hpi. RNA-seq was conducted using Illumina HiSeq4000 sequencing system. For RNA-seq analysis, all of the raw reads were filtered by Fastp (version 0.18.0) software to remove adapters and low quality reads (quality score ≤ 20) (41). Clean reads were aligned to the reference genome of Fg strain PH-1 (assembly ASM24013v3) using Hisat2 (v1.3.3) (42). Expression levels for each sample were quantified to FPKM (fragment per kilobase of transcript per million mapped reads) using Stringtie (v1.2.0) (43). Genes displaying log_2[fold change] ≥1.5 and an adjusted (false discovery rate) *P* value <0.05 were classified as differentially expressed genes (DEGs) by using DESeq2 package (44).

For RT-qPCR assay, the concentrations of purified RNA samples were determined with the Nanodrop 8000 spectrophotometer. Five micrograms of total RNA were reverse transcribed using Primescript™ first-Strand cDNA synthesis system (TaKaRa, Dalian, China) with an oligo(dT) primer and cDNA was quantified in real-time PCR using TB Green Fast qPCR Mix kit (TaKaRa, Dalian, China). Quantitative PCR reactions were performed in 20 μl in 96-well plates on a ABI QuantStudio™ 5 machine (ThermoFisher Scientific, Waltham, USA) and with the following cycling conditions: 95°C/30 s and then 40 cycles of 95°C/5 s, 60°C/15 s. All of the measurements were followed by melting curve analysis. Results were analyzed using QuantStudio™ 5 machine (ThermoFisher Scientific, Waltham, USA). The comparative cycle threshold (CT) method was used for data analysis and relative fold difference was expressed as $2^{-\Delta\Delta CT}$. As an internal control, primers for *FgACTIN* were used for each quantitative real-time PCR analysis. Primer sequences used for RT-qPCR are listed in Supplementary Table S1.

Chromatin immunoprecipitation (ChIP)-seq and ChIP-qPCR analyses

ChIP was performed according to a previously described protocol with minor modifications (45). Briefly, fresh mycelia of each sample were cross-linked with 1% formaldehyde for 10 min. Fixation was stopped with 125 mM glycine for 5 min. Subsequently, fixed culture samples were grounded in liquid nitrogen, and re-suspended in 10 ml of

nuclear extraction buffer I (0.4 M sucrose, 10 mM Tris–HCl, pH 8.0, 10 mM $MgCl_2$, 5mM β-mercaptoethanol, 0.1 mM PMSF, 1× protease inhibitor). DNA was sheared into 200–500 bp fragments with 30 s on and 6 min off by using a Covaris E220 DNA Sonicator (Covaris, Woburn, MA). After centrifugation, the pellets were suspended in 4 ml of nuclear extraction buffer II (1.7 M sucrose, 10 mM Tris–HCl, pH 8.0, 10 mM $MgCl_2$, 1% Triton X-100, 5 mM β-mercaptoethanol and 1× protease inhibitor). Re-suspended samples were then centrifuged at 13 000 × *g* for 15 min at 4°C. The resulting pellets were re-suspended in 300 µl of nuclear lysis buffer (50 mM Tris–HCl, pH 8.0, 10 mM EDTA, 1% SDS and 1 × protease inhibitor). Samples were then sonicated by two pulses of 30 s sonication and 1 min rest. After centrifugation at 4000 × *g* for 5 min at 4°C, the supernatant was transformed into a clear tube, and was diluted with 10 × ChIP dilution buffer (1.1% Triton X-100, 1.2 mM EDTA, 16.7 mM Tris–HCl, pH 8.0 and 167 mM NaCl). Immunoprecipitation was conducted using the monoclonal anti-GFP (ab290, Abcam, Cambridge, UK) antibody, anti-H3K18ac (39755, Active Motif Inc., Carlsbad, USA) antibody, or anti-H2BK11ac (ab240613, Abcam, Cambridge, UK) together with the protein A agarose beads (sc-2003, Santa Cruz, CA, USA). The beads were subsequently washed by low salt wash buffer, high salt wash buffer, LiCl wash buffer, and TE buffer. After washing, eluting, reversing the crosslinking, and removing all proteins, the resulting pellets were re-suspended in 50 µl of distilled water. DNA was extracted by phenol/chloroform method. As controls, input DNA was recovered by phenol extraction after the sonication step. The DNA extracted from the FgPacC30-GFP ChIP samples was subjected to high-throughput sequencing on the Illumina Hiseq4000 platform by BGI (Shenzhen, China). Two biological replicates were included for each ChIP-seq assay.

For ChIP-seq analysis, 50 bp single-end reads of ChIP-seq were obtained, and the quality was controlled using SOAPnuke (v2.1.7) (46). The parameters were used as follows: remove the reads containing adapters or >1% of unknown nucleotides (N); delete the reads if there are >40% bases having a quality value lower than 20. Clean reads were mapped to the reference genome of Fg strain PH-1 (assembly ASM24013v3) by Bowtie2 (version 2.4.5) with default parameters. RPKM (reads per kilobase per million mapped reads) were calculated to normalized reads using bamCompare tool in Deeptools (version 2.4.1) with input DNA as a control (47–48). Visualization of the average read coverage over 2 kb upstream and downstream of the TSS was performed by Deeptools. BigWig files generated by Deeptools were used for visualization in Integrative Genome Viewer (version 2.8.9) (49).

The PCR primers used for ChIP-qPCR assays are listed in Supplementary Table S1. Relative enrichment values were calculated by dividing the amount of immunoprecipitated DNA by the amount of input DNA.

Co-immunoprecipitation and affinity capture-mass spectrometry analysis

For *in vivo* co-immunoprecipitation (co-IP) assays, constructs of targeted genes fused with different markers (GFP, 3 × Flag) were transformed in pairs into the wild-type PH-1. The resulting transformants were confirmed by western blot analysis with monoclonal anti-Flag (F1804, Sigma-Aldrich, St. Louis, MO, USA) and anti-GFP (ab32146, Abcam, Cambridge, UK). Total proteins from the strain bearing a pair of fusion constructs were extracted, and were further incubated with the anti-GFP agarose (ChromoTek, Martinsried, Germany) at 4°C overnight. Proteins eluted from the agarose were analyzed by western blot with the anti-FLAG antibody. The protein samples were also detected with the monoclonal anti-GAPDH antibody (EM1101, HuaAn Biotech. Ltd., Hangzhou, China) as a reference. All western blots were recorded and imaged by Image Quant LAS4000 mini (GE Healthcare, Chicago, USA). To perform affinity capture-mass spectrometry analysis, the functional isoform FgPacC (FgPacC30) was tagged with GFP and transformed into the ΔFgPacC mutant. The resulting transformant ΔFgPacC::FgPacC30-GFP was used for affinity capture-mass spectrometry analysis as described previously (31). Furthermore, ΔFgPacC transformed with GFP fragment was used as a control for exclusion of nonspecific affinity proteins.

Yeast two-hybrid (Y2H) and microscale thermophoresis (MST) assays

To construct plasmids for yeast two hybrids (Y2H) analysis, the coding sequence of each gene was amplified from cDNA of the wild-type strain PH-1 with corresponding primer pairs indicated in Supplementary Table S1. Each cDNA fragments were cloned into the yeast GAL4-binding domain vector pGBKT7 and GAL4-activation domain vector pGADT7 (Clontech, Mountain View, CA, USA), respectively. Pairs of Y2H plasmids were co-transformed into *S. cerevisiae* strain AH109 following the LiAc/SS-DNA/PEG transformation protocol. In addition, the plasmid pair pGBKT7-53 and pGADT7-T was served as a positive control. The plasmid pair pGBKT7-Lam and pGADT7-T was used as a negative control. Transformants were grown at 30°C for 3 days on synthetic medium (SD) lacking Leu and Trp, and then transferred to SD without His, Leu, Trp and Ade to assess protein-protein interaction. Three independent experiments were assayed to confirm each Y2H result.

Microscale thermophoresis (MST) assays were performed by using Monolith NT.115 (NanoTemper Technologies, Germany) as described in previous publications (50). Target proteins were fluorescently labeled with NT-647-NHS (NanoTemper Technologies) via amine conjugation. For detecting the binding affinity, 10 µM of fluorescently labeled protein in label buffer (130 mM $NaHCO_3$, 50 mM NaCl) was titrated against increasing concentrations of unlabeled ligand. The samples were loaded into MST premium-coated capillaries (Monolith NT.115 MO-K005, Germany) and measured at 25°C with 80% MST power and and 20% LED power. Data were analyzed using Nano Temper Analysis Software (NanoTemper Technologies, Germany).

HAT activity assays

An *in vitro* histone acetylation assay was carried out following a previous publication with minor modifications

(51). Briefly, purified histone proteins (H3-His and H2B-His) was incubated with purified FgGCN5-His protein in HAT buffer (50 mM pH 8.0 Tris–HCl, 50 mM KCl, 0.1 mM EDTA, 1 mM DTT, 1 mM protease inhibitor, 5% glycerol, and 5 mM acetyl-CoA) in the absence or presence of increasing concentrations of FgPacC30-His protein. The resulting reactions were then resolved by SDS-PAGE and analyzed by western blotting using anti-H3K18ac (39755, Active Motif Inc., Carlsbad, USA), anti-H2BK11ac (ab240613, Abcam, Cambridge, UK) antibodies.

Phos-tag analysis

The FgPacC30-Flag fusion construct was transformed into the wild-type strain PH-1 and the mutant ΔFgHal4, respectively. Proteins of the resulting strains were resolved on 8% SDS-polyacrylamide gels supplemented with 25 μM Phos-binding reagent acrylamide (F4002, APE × BIO) and 100 μM $ZnCl_2$. Gels were first equilibrated three times in transfer buffer containing 5 mM EDTA for 5 min and further equilibrated in transfer buffer without EDTA twice for 5 min. Proteins from the Zn^{2+}-phos-tag acrylamide gel to the PVDF membrane were transferred for 4 h at 100 V. Finally, the transferred membrane was analyzed via western blotting with the anti-Flag antibody.

Electrophoretic mobility shift assay (EMSA) and luciferase activity assays

For determination of the binding ability of FgPacC30 with the potential element GCCAR(R = A/G)G, FgPacC30 was amplified and cloned into pET32a vector to generate the recombinant FgPacC30-His protein in *E. coli* BL21. FgPacC30-His was further purified by Ni Sepharose beads and eluted by imidazole (Supplementary Figure S2). The biotin-labeled DNA probes were synthesized by GenScript (Nanjing, China). The EMSA assay was performed using a LightShift™ Chemiluminescent EMSA Kit (20148, Thermofisher, USA) following the manufacturer's instruction (52). Briefly, purified FgPacC30-His was mixed with biotin-labeled or competitive probes, and then inoculated for 20 min at 25°C. The reaction mixtures were separated on a 6% polyacrylamide mini gel for 90 min, and then transferred to a positively charged nylon membrane (Millipore, USA). Signals were visualized using Image Quant LAS4000 mini (GE Healthcare, Chicago, USA).

For luciferase activity assay, the promoter fragments of *FgNPS6*, *FgSID1*, *FgMIRB*, *FgSIT1*, *FgHAPX* and *FgSREA* were cloned into LUC reported plasmid pICSL86900. The full-length sequence of FgPacC30-GFP was inserted into pICH86988 vector. The resulting constructs were transformed into *Agrobacterium* GV3101 cells, and then co-expressed or separately expressed in *Nicotiana benthamiana*. To capture LUC images, *N. benthamiana* leaves were sampled after infiltration at 48 hours. The samples were incubated with 1 mM luciferin substrate (Biovision, San Francisco, America), and then photographed under a Tanon-6600 Multi Chemiluminescent Imaging System (Tanon, Shanghai, China). The LUC activity of each sample was quantified with a Promega GloMax Navigator microplate luminometer.

Bimolecular fluorescence complementation (BiFC) assay

The FgPacC30-CYFP fusion constructs were constructed by cloning the fragments into pHZ68. Meanwhile, the FgHal4-NYFP or FgGcn5-NYFP fusion constructs were generated by cloning the related fragments into pHZ65. A pair of FgPacC30-CYFP and FgHal4-NYFP or FgGcn5-NYFP constructs was co-transformed into the protoplasts of wild type PH-1. YFP signals were examined under a Zeiss LSM710 confocal microscope (Gottingen, Niedersachsen, Germany). The nuclear localization was confirmed by simultaneous nuclear staining with 4′-6-Diamidino-2-phenylinodle (DAPI).

RESULTS

Fg infection provokes iron accumulation in wheat tissues

Alkalinization of host tissues has been reported from several hemibiotrophic pathogens including *Colletotrichum* species and *Fusarium oxysporum* to increase their infectious potential and suppress host immunity during the early biotrophic stages of infection (53–55). Thus, we initiated this project to investigate the pH changes during Fg infection. Firstly, we adapted a bioassay in plates containing different pH indicators, and observed significant extracellular alkalinization surrounding the wheat seedling leaves and roots infected with Fg (Supplementary Figure S3). By using a previously reported apoplastic pH fluorescent indicator 8-hydroxypyrene-1,3,6-trisulfonic acid trisodium salt (HPTS) (37,38), we found that pH upshifts in the apoplast of wheat seedling leaves started at 48 hours post-inoculation (hpi), and increased significantly at 120 hpi (Figure 1A, B). Then, we sought to monitor the pH dynamics in the apoplastic fluids from wheat tissues over time in response to Fg infection with a pH electrode. At 48 hpi, the pH in the apoplast of wheat heads and seedling leaves presented a slight upshift with an average of 5.3 ± 0.3 and 5.6 ± 0.3, respectively (Figure 1C). The pH values increased rapidly after 48 hpi, and reached 7.9 ± 0.4 and 8.3 ± 0.1 at 120 hpi for the infected wheat heads and seedling leaves, respectively (Figure 1C). In contrast, the apoplastic pH of uninfected controls remained at $4.9–5.0 \pm 0.3$ at 120 hpi (Figure 1C). These data indicate that Fg infection is able to induce rapid extracellular alkalinization in wheat tissues during 48–120 hpi, which verifies the previous finding from *F. oxysporum* and *Colletotrichum* spp.

To explore potential effects of host alkalinization on Fg pathogenesis, we investigated transcription profiling using the RNA-sequencing (RNA-seq) approach for Fg *in vitro* (representing 0 hpi) and *in planta* at 24, 48 and 120 hpi, respectively. Principle component analysis showed that the transcriptomes of Fg grown *in planta* at acid conditions (at 24 or 48 hpi) were more similar to each other, but different from that at alkaline pH condition (at 120 hpi) (Supplementary Figure S4A, B), implying a transcriptional reprogramming in Fg during host alkalinization. Next, we analyzed the genes whose expressions were significantly changed during plant alkalinization. Interestingly, gene ontology (GO) enrichment analysis showed that the expression levels of genes related to iron acquisition pathways, including siderophore metabolism and transport, as well
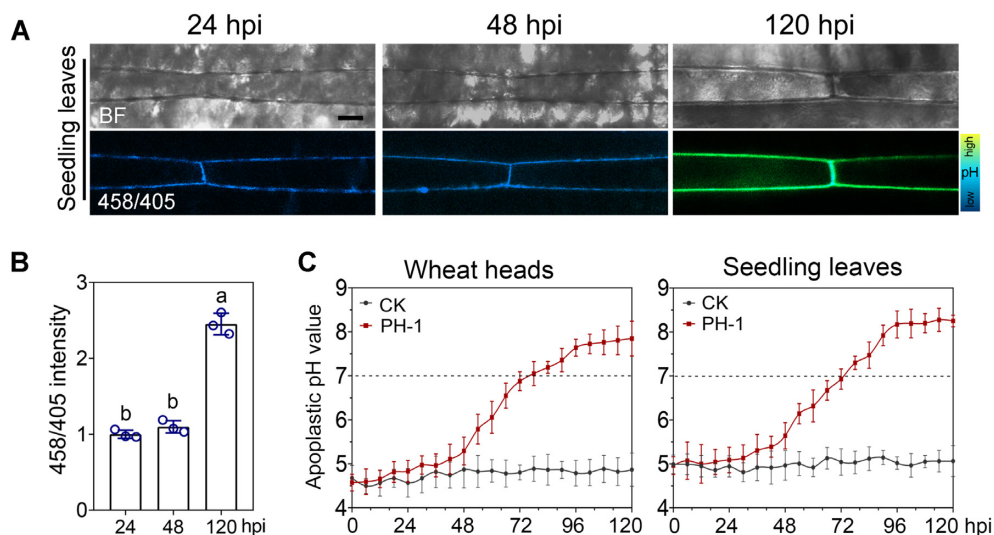
Figure 1. *F. graminearum* infection provokes host alkalinization. (**A**) Time-course images of pH upshifts in the apoplast of wheat seedling leaves during *F. graminearum* (Fg) infection. HPTS (8-hydroxypyrene-1,3,6-trisulfonic acid trisodium salt) staining showed the apoplastic pH changes of wheat seedling leaves inoculated with Fg at 24, 48 and 120 h post-inoculation (hpi). Ratiometric images taken by using a confocal indicate the intensity of 458 nm divided by the intensity of 405 nm for each pixel. Scale bar: 20 μm. (**B**) Quantification of the intensity of 458/405 nm values in wheat seedling leaves inoculated with Fg at 24, 48 and 120 hpi. Data are presented as the mean ± standard deviation from three biological replicates. Different letters (a, b) represent significant differences statistically according to the one-way ANOVA followed by Fisher's LSD test ($P < 0.05$). (**C**) The pH levels in apoplastic fluid samples from the palea tissues of wheat spikelets and seedling leaves at different time points after inoculation with Fg. Data are presented as the mean ± standard deviation from six replicates for each time point.

as reductive iron assimilation (RIA), were suppressed at 120 hpi as compared with those at 24 and 48 hpi (Figure 2A). Previous studies have shown that the siderophore-mediated iron uptake is the major pathway for fungal iron acquisition in Fg (56,57). Therefore, we generated the deletion mutants of the key siderophore biosynthesis (*FgNPS6* and *FgSID1*) and transport genes (*FgSIT1* and *FgMIRB*), and found that all of these Fg mutants exhibited defects in iron uptake (Supplementary Figure S5), confirming previous findings (56,57). Then, we further examined the expression of these iron uptake genes at 24, 48 and 120 hpi by quantitative reverse transcription PCR (RT-qPCR) (Figure 2B), and found that they were transcriptionally repressed during plant alkalinization (48–120 hpi). Collectively, these results indicate the expression of iron uptake genes in Fg are suppressed during host alkalinization.

Previous studies in filamentous fungi have showed that expression of iron uptake genes were inhibited under high-iron stress (58). Given that the expression of iron uptake genes in Fg are suppressed after 48 hpi, we proposed that Fg might face high-iron stress during its infection. To test this hypothesis, we determined iron dynamics in wheat tissues in response to Fg infection by using the Fe^{2+} indicator FeRhoNox™-1. As shown in Figure 2C and Supplementary Figure S6, abundant iron significantly accumulated in the apoplast of wheat seedling leaves at 48 to 120 hpi, but not at 24–48 hpi. Furthermore, we determined the apoplastic iron content of wheat seedling leaves at 24, 48 and 120 hpi. The iron concentration accumulated approximately to 5 mM at 120 hpi that was significantly higher than those at 24 and 48 hpi (Figure 2D). Taken together, these data reveal that Fg infection provokes iron accumulation in wheat tissues.

Previous studies have reported that many plants are able to locally accumulate iron to inhibit pathogen infectious growth (5,10,11). To further evaluate effects of high-iron stress on Fg growth during its infection under different pH levels, the wild-type strain PH-1 was grown on solid high-iron media (5 mM Fe^{2+}) buffered to pH 4.0, 6.5 and 8.0, respectively. Unexpectedly, Fg growth was inhibited on solid high-iron media at pH 4.0 and 6.5 conditions; however, Fg was hypertolerance to high-iron stress under pH 8.0 condition (Figure 3A). These results support a mechanism for Fg to tolerate high-iron stress under alkaline host environment during infection.

FgPacC serves as a major regulator for high-iron stress response in Fg under alkaline host environment

Next, we aimed to elucidate regulatory mechanisms of Fg adaption to high-iron stress under alkaline host environment. As previously reported in filamentous fungi *Aspergillus* spp. and *Alternaria alternata*, two transcription factors SreA and HapX serve as key regulators for fungal adaption to iron excess (59–62). Therefore, we generated *FgHAPX* and *FgSREA* deletion mutants, and determined their sensitivity to high-iron stress at different pH levels. Phenotypic analysis showed that FgHapX- or FgSreA-deficiency rendered Fg more susceptible to high-iron stress than wild-type PH-1 only under acid or neutral conditions, but not at alkaline pH condition (Figure 3A, B), indicating that Fg may contain a FgHapX- and FgSreA-independent regulatory mechanism mediating response of the pathogen to high-iron stress during plant alkalinization.

From the transcriptome data and RT-qPCR assay, we found that expression of the pH responsive transcriptional regulator *FgPACC* (FGSG_12970) was induced dur-
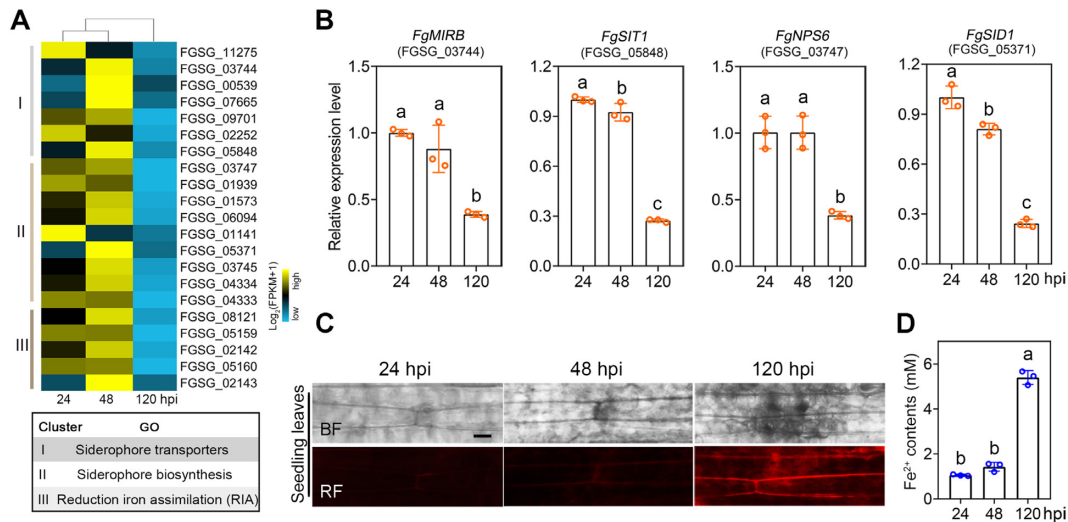
Figure 2. The expression of iron uptake genes in *F. graminearum* is repressed during host alkalinization. (**A**) Hierarchical clustering of 21 iron uptake genes at 120 hours post-inoculation (hpi) as compared with those at 24 or 48 hpi. Colors represented the $\log_2$(FPKM + 1) of the iron uptake genes (upper panel). A list of GO terms enriched in the clusters is shown (lower panel). (**B**) Expression of *FgMIRB*, *FgSIT1*, *FgNPS6* and *FgSID1* at 24, 48, and 120 hpi was evaluated by RT-qPCR using *FgACTIN* gene as the internal control. Expression of each iron uptake gene at 24 hpi was set as 1.0. Data are presented as the mean ± standard deviation from three biological replicates. Different letters (a, b and c) represent significant differences statistically according to the one-way ANOVA followed by Fisher's LSD test ($P < 0.05$). (**C**) Time-course images of the iron accumulation in wheat seedling leaves during Fg infection. FeRhoNox™-1 (red fluorescence) staining showed ferrous iron (Fe^{2+}) accumulation in the apoplasts of wheat seedling leaves. Scale bar: 20 μm. (**D**) Ferrous iron (Fe^{2+}) contents in apoplastic fluid samples from wheat seedling leaves inoculated with Fg at 24, 48 and 120 hpi. Data are presented as the mean ± standard deviation from three biological replicates. Different letters (a, b) represent significant differences statistically according to the one-way ANOVA followed by Fisher's LSD test ($P < 0.05$).

ing host alkalinization (48–120 hpi) (Figure 3C). We therefore generated the *FgPACC* knock out mutant ΔFgPacC and found that the mutant exhibited significantly increased sensitivity to high-iron stress at alkaline pH condition (Figure 3A, B; Supplementary Figure S1). To elucidate whether FgPacC controls the expression of iron uptake genes in Fg, we profiled the transcriptome of ΔFgPacC at pH 8.0 condition, and found that iron uptake related genes, encoding for siderophore metabolism and transport proteins, iron permease, and RIA (reductive iron assimilation) proteins were significantly up-regulated in the mutant (Figure 3D). RT-qPCR assays confirmed that the transcript levels of key iron uptake genes, *FgNPS6*, *FgSID1*, *FgSIT1* and *FgMIRB*, were significantly increased in ΔFgPacC under alkaline condition (Figure 3E). Collectively, these results indicate that FgPacC could repress the expression of iron uptake genes in Fg, thus conferring the adaption of the fungus to high-iron stress at alkaline pH condition.

In order to determine whether FgPacC-dependent high-iron resistance during plant alkalinization is important for fungal virulence of Fg, we examined the pathogenicity of ΔFgPacC. The results showed that the disease index of ΔFgPacC on wheat spikelets was significantly decreased as compared with those of the wild-type PH-1 and complementary strain ΔFgPacC::FgPacC (Figure 3F, G). Moreover, we also found that the lesion area on wheat seedling leaf caused by ΔFgPacC was significantly reduced at 120 hpi, but not at 48 hpi (Figure 3H). Taken together, these findings indicate that FgPacC is required for full virulence of Fg.

FgPacC is cleaved into a functional isoform during plant alkalinization, that binds to the promoters of iron uptake genes of Fg

Previous studies have revealed that fungal PacC must undergo alkaline pH-dependent proteolytic cleavage into the functional isoform, and thereby translocating into nucleus and orchestrating the cellular response to pH upshifts (63). To examine the processing and subcellular localization of FgPacC in Fg, GFP was fused to the N-terminal of FgPacC driven by the FgPacC native promoter. The resulting *GFP::FgPACC* construct was then transformed into the ΔFgPacC mutant to generate the complementary strain ΔFgPacC::GFP-FgPacC. We found that GFP-FgPacC was rapidly translocated into nucleus, and cleaved into a 30-kDa active form (named FgPacC30 thereafter) under alkaline pH condition (Supplementary Figure S7A, B), similar to the size reported for other fungi (63,64). To characterize functions of the isoform FgPacC30, we complemented the mutant ΔFgPacC with FgPacC30 fused with GFP under the control of its native promoter to construct a complementary strain ΔFgPacC::FgPacC30-GFP. Phenotypic assays showed that FgPacC30-GFP was exclusively localized to the nucleus even at acidic conditions, and could fully complement the defects of ΔFgPacC in high-iron resistance under alkaline condition (Supplementary Figure 7A, C). Bioinformatic analysis revealed that a predicted nuclear localization sequence (NLS) was located in the N-terminal of FgPacC30. To evaluate whether the nuclear localization is essential for FgPacC30 function, we complemented ΔFgPacC with a mutated FgPacC30-GFP without the NLS domain (ΔFgPacC::FgPacC30$^{\Delta NLS}$-GFP). As
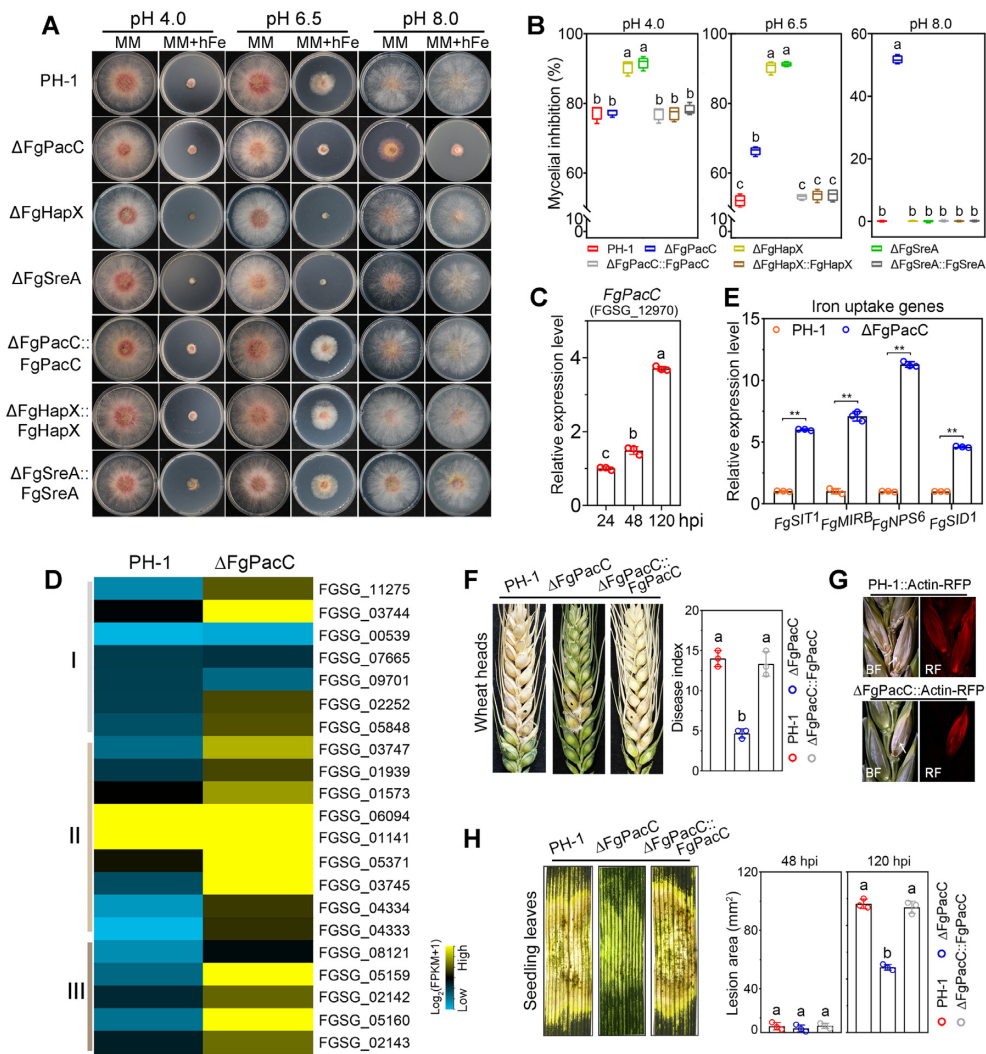
Figure 3. FgPacC mediates high-iron resistance by repressing the expression of iron uptake genes during fungal infection. (**A**) ΔFgPacC exhibited increased sensitivity to high-iron stress at pH 8.0. The sensitivity of wild-type PH-1, the mutants (ΔFgPacC, ΔFgHapX, and ΔFgSreA), and the complementary strains (ΔFgPacC::FgPacC, ΔFgHapX::FgHapX, and ΔFgSreA::FgSreA) to high-iron stress was determined at pH4.0, 6.5 or 8.0. A five-mm mycelial plug of each strain was incubated for three days on minimal medium (MM) supplement with or without 5 mM Fe^{2+} at pH 4.0, 6.5 or 8.0. (**B**) Mycelial inhibition by the high-iron stress relative to each untreated control was calculated for each strain at pH 4.0, 6.5 and 8.0, respectively. Data are presented as the mean ± standard deviation from four biological replicates. Different letters (a, b and c) represent significant differences statistically according to the one-way ANOVA followed by Fisher's LSD test ($P < 0.05$). (**C**) Expression of *FgPACC* at 24, 48 and 120 hpi was evaluated by RT-qPCR using *FgACTIN* gene as the internal control. *FgPACC* expression at 24 hpi was set as 1.0. Data are presented as the mean ± standard deviation from three biological replicates. Different letters (a, b and c) represent significant differences statistically according to the one-way ANOVA followed by Fisher's LSD test ($P < 0.05$). (**D**) Heatmap showed the iron uptake genes regulated by FgPacC in the mutant ΔFgPacC as compared to those the wild-type PH-1 in RNA-seq assays. Colors represented the $\log_2$(FPKM + 1) of the differentially expressed iron uptake genes. Yellow color indicates relatively high expression, and green color indicates relatively low expression. (**E**) The expression levels of iron uptake genes were evaluated by RT-qPCR in the wild-type PH-1 and the mutant ΔFgPacC at pH 8.0 using *FgACTIN* gene as the internal control. Expression of each iron uptake gene in wild-type PH-1 was set as 1.0. Data are presented as the mean ± standard deviation from three biological replicates. Statistical significance compared to the wild-type PH-1 was determined using Student's *t*-test (**$P < 0.01$). (**F**) Virulence of the wild-type PH-1, the mutant ΔFgPacC, and the complementary strain ΔFgPacC::FgPacC were evaluated on wheat heads. Images of infected wheat heads were photographed at 14 dpi (left panel). The mean and standard deviation of the disease index of each strain were estimated with data from three independent replicates (right panel). Different letters (a, b) represent significant differences statistically according to the one-way ANOVA followed by Fisher's LSD test ($P < 0.05$). (**G**) Cross-sections of inoculated and adjacent wheat spikelets. Spikelets were infected with PH-1::FgActin-RFP or ΔFgPacC::FgActin-RFP. The samples were taken at 7 dpi. Inoculated spikelets are indicated with white arrows. (**H**) Virulence of the wild-type PH-1, the mutant ΔFgPacC, and the complementary strain ΔFgPacC::FgPacC were evaluated on seedling leaves. Images of infected seedling leaves were photographed at 120 hpi (left panel). Lesion area caused by each strain was measured at 48 hpi and 120 hpi, respectively (right panel). Data are presented as the mean ± standard deviation from three biological replicates. Different letters (a, b) represent significant differences statistically according to the one-way ANOVA followed by Fisher's LSD test ($P < 0.05$).

shown in Supplementary Figure 7C, FgPacC30$^{\Delta NLS}$-GFP was unable to accumulate in the nucleus, and the strain ΔFgPacC::FgPacC30$^{\Delta NLS}$-GFP lost the function of high-iron resistance at alkaline pH condition. Therefore, these results indicate that the proteolytic cleavage and nuclear localization of FgPacC is required for high-iron resistance of Fg under alkaline host environment.

Next, we performed chromatin immunoprecipitation-quantitative PCR (ChIP-qPCR) assay with ΔFgPacC::GFP-FgPacC under acidic (pH 4.0) and alkaline (pH 8.0) conditions. The results showed that GFP-FgPacC was significantly enriched at the promoters of iron uptake genes *FgNPS6*, *FgSID1*, *FgSIT1*, *FgMIR*B, *FgSIDF* and *FgFETC* at pH 8.0, but not at pH 4.0 (Figure 4A), indicating that FgPacC binds to the promoters of iron uptake genes at alkaline condition. Since FgPacC undergoes a C-terminal cleavage and nuclear translocation at alkaline condition, we further examined whether the FgPacC30 isoform could direct bind to the promoters of iron uptake genes. ChIP-qPCR assays with ΔFgPacC::FgPacC30-GFP revealed that the functional isoform FgPacC30 could bind to the promoters of iron uptake genes, at both pH 4.0 and pH 8.0 conditions (Figure 4B). Dual-LUC assays verified the binding of FgPacC30 with the promoters of these iron uptake-related genes *in planta* (Supplementary Figure S8). To further evaluate whether other iron uptake-related genes are also regulated by FgPacC30, we performed a genome-wide ChIP-Seq assay with ΔFgPacC::FgPacC30-GFP, and found that FgPacC30 bound to the promoter regions of 14 genes involved in fungal iron uptake (Supplementary Figure S9).

Previous studies showed that the functional PacC isoform could bind to a *cis*-element GCCAR(R = A/G)G ([65],[66]). The multiple EM for motif elicitation (MEME) analysis showed that all of these FgPacC-targeted iron uptake-related genes harbor this conserved PacC-binding *cis*-element (Figure 4C). Therefore, we purified the functional form FgPacC30 fused with 6 × His (named FgPacC30-His) to detect its binding ability to this consensus by using EMSA. As shown in Figure 4D, FgPacC30-His was able to bind to 6 × GCCAR(R = A/G)G, whereas excess unlabeled fragments blocked the binding, underlining specificity of the binding of FgPacC30 with GCCAR(R = A/G)G. Moreover, microscale thermophoresis (MST) analysis further verified the binding of FgPacC30 with 6 × GCCAR(R = A/G)G element (Figure 4E). Taken together, these results indicate that FgPacC30 directly binds to the GCCAR(R = A/G)G element at the promoters of genes involved in iron uptake and suppresses their transcription.

FgPacC30 binds to FgGcn5 and downregulates histone acetylation in Fg

To understand the molecular mechanism of FgPacC30 in repressing the expression of iron uptake-related genes, we tried to identify FgPacC30-interacting proteins in Fg by performing the affinity capture assay using FgPacC30-GFP as a bait. The wild-type strain PH-1 expressing GFP was used as a negative control. Given that FgPacC30 is localized to nucleus and represses gene expression, we scanned for the FgPacC30-interacting proteins that are potentially

nuclear localized. Among the 41 candidates, we found that FgPacC30 might interact with FgGcn5, a homolog of *S. cerevisiae* Gcn5 (Supplementary Table S2), which is a catalytic subunit of SAGA complex. The association of FgPacC30 with FgGcn5 was further confirmed via co-immunoprecipitation (co-IP) and yeast two hybrids (Y2H) (Figure 5A, B). MST tests also revealed a strong binding affinity of FgPacC30 with FgGcn5 (Figure 5C). Moreover, the bimolecular fluorescence complementation (BiFC) assays showed that functional isoform FgPacC30 interacted with FgGcn5 in the nucleus (Figure 5D).

Because FgPacC30 physically interacted with FgGcn5, we next examined the effect of FgPacC deletion on FgGcn5-mediated histone acetylation in Fg. As reported previously, FgGcn5 is essential for acetylation of H3K18 and H2BK11 (named as H3K18ac and H2BK11ac, respectively) ([26]). Therefore, we evaluated H3K18ac and H2BK11ac levels in ΔFgPacC. Notably, we found that H3K18ac and H2BK11ac levels were enhanced in ΔFgPacC as compared to those in the wild-type PH-1 (Figure 5E). Moreover, Y2H assays showed that the acetyltransferase (HAT) domain of FgGcn5 was required for its interaction with FgPacC30 (Supplementary Figure S10). These results imply that Fg-PacC30 may directly inhibit the HAT activity of FgGcn5, and subsequently reduce histone acetylation. To verify this possibility, we evaluated the effect of FgPacC30 on the acetyltransferase activity of FgGcn5 on histone protein H3 and H2B *in vitro*. The FgGcn5-, H3-, and H2B-6 × His proteins were purified with a Ni-NTA column. As shown in Figure 5F, FgGcn5 was able to catalyze the acetylation of H3K18 and H2BK11. Importantly, both the levels of H3K18ac and H2BK11ac were notably decreased in the presence of FgPacC30 at different molar ratios (3×, and 6 × in relative to FgGcn5) (Figure 5F), indicating that Fg-PacC30 was able to directly inhibit the HAT activity of Fg-Gcn5 *in vitro*. Taken together, these results demonstrate that FgPacC30 binds FgGcn5 to deregulate the histone acetylation in Fg.

FgPacC30 represses expression of iron uptake genes by reducing FgGcn5-mediated histone acetylation during infection

To investigate the potential roles of FgGcn5-mediated histone acetylation in expression of iron uptake genes, we generated the deletion mutants of FgGcn5, and found that ΔFgGcn5 showed the defects of global acetylation of H3K18 and H2BK11 (Supplementary Figure S11A). ChIP-qPCR assays showed that the lack of FgGcn5 led to significantly decreased H3K18ac or H2BK11ac enrichments at the promoters of iron uptake genes (*FgNPS6*, *FgSID1*, *FgSIT1* and *FgMIRB*) as compared to those of the wild type under alkaline and high-iron condition (Figure 6A). Accordingly, RT-qPCR results showed that the deletion of FgGcn5 led to the low expression levels of these iron uptake genes under alkaline and high-iron conditions (Supplementary Figure S11B). Collectively, these results suggest that FgGcn5-mediated histone acetylation contributes to the transcriptional activation of iron uptake genes in Fg.

As reported in *S. cerevisiae*, Gcn5 forms a HAT module with Ada2 and Ada3, which is required for the SAGA's nucleosomal HAT activity ([67–69]). *In vivo* co-IP and *in vitro*
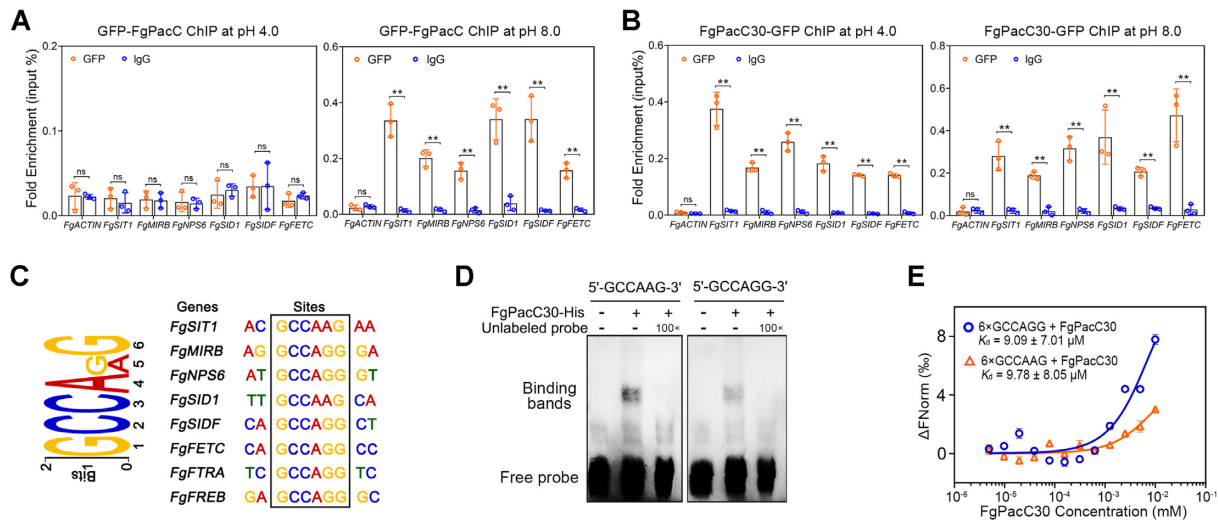
Figure 4. FgPacC30 binds to a conserved motif GCCAR(R = A/G)G at the promoters of genes involved in iron uptake. (A, B) ChIP-qPCR assays revealed the enrichment of GFP-FgPacC (**A**) and FgPacC30-GFP (**B**) at the promoters of the *FgNPS6*, *FgSID1*, *FgSIT1*, *FgMIRB*, *FgSIDF* and *FgFETC* genes at pH 4.0 and pH 8.0. ChIP- and input-DNA samples were quantified by quantitative PCR assays with the primer pair indicated in Supplementary Table S1; rabbit IgG was used as a negative control. Data are presented as the mean ± standard deviation from three biological replicates. Statistical significance compared to IgG was determined using Student's *t*-test (ns: not significant, **P < 0.01). (**C**) Identification of FgPacC30 binding motifs by using the multiple EM for motif elicitation (MEME) program. The identified binding *cis*-element in iron metabolism genes were indicated in the black square. (**D**) FgPacC30 bound to the *cis*-element GCCAR(R = A/G)G in electrophoretic mobility shift assay (EMSA). The binding of PacC30-His with the biotin-labeled 6 × GCCAAG or 6 × GCCAGG was determined by EMSA. The 100-fold excess of unlabeled element was used as competitors. (**E**) Microscale thermophoresis (MST) assays showed the binding of FgPacC30 with 6 × GCCAAG or 6 × GCCAGG. The dissociation curve was fit to the data to calculate the K_d values. Data are presented as the mean ± standard deviation from three repeated experiments.

MST assays showed that both FgAda2 and FgAda3 can interact with FgGcn5 (Supplementary Figure S11C, D). FgAda2 and FgAda3 deletion mutants showed similar defects with ΔFgGcn5 in histone acetylation at H3K18 and H2BK11 (Supplementary Figure S11A). RT-qPCR assays also revealed that both FgAda2 and FgAda3 promoted expression of iron uptake genes under alkaline and high-iron condition (Supplementary Figure S11E). These results indicate that SAGA complex plays an important role in transcriptional regulation of iron uptake genes in Fg.

Given that FgGcn5-mediated H3K18ac and H2BK11ac are associated with expression of iron uptake genes, and FgPacC30 is able to inhibit the HAT activity of FgGcn5, we speculated that FgPacC represses these genes expression through its inhibition on FgGcn5-mediated histone acetylation. To test this hypothesis, we determined impact of FgPacC deletion on H2BK11ac and H3K18ac enrichment at the key iron uptake genes, *FgNPS6*, *FgSID1*, *FgSIT1* and *FgMIRB*. The results showed that, compared with the wild-type PH-1, ΔFgPacC exhibited significantly higher enrichments of H3K18ac and H2BK11ac in these iron uptake genes after incubation for 6 and 9 h under alkaline and high-iron conditions, but showed no obvious changes under acidic and low-iron conditions (Figure 6A), indicating that FgPacC downregulates the histone acetylation on iron uptake genes under alkaline and high-iron condition. Next, we generated the double deletion mutant (ΔFgPacC + FgGcn5) and the RT-qPCR assays showed that the expression levels of iron uptake genes were significantly decreased in ΔFgGcn5 and ΔFgPacC + FgGcn5 as compared with those in wild-type PH-1 at alkaline and high-iron conditions (Supplementary Figure S11B). ChIP-

qPCR assays also revealed that both ΔFgPacC + FgGcn5 and ΔFgGcn5 exhibited similar decreased enrichments of H3K18ac and H2BK11ac at iron uptake genes (Figure 6A). Collectively, these findings support that FgPacC suppresses iron uptake genes expression under alkaline and high-iron conditions through inhibition of FgGcn5-mediated histone acetylation at iron uptake genes. Notably, although ΔFgGcn5 and ΔFgPacC + FgGcn5 displayed significantly decreased sensitivity to high-iron stress under alkaline condition as compared with ΔFgPacC, they exhibited stronger defects in mycelial growth without high-iron treatment (Supplementary Figure S11F). Moreover, ΔFgGcn5 and ΔFgPacC + FgGcn5 displayed stronger defects in virulence on wheat heads than ΔFgPacC (Supplementary Figure S11G), indicating that FgGcn5 may have both positively and negatively regulatory roles in mycelial growth and virulence, acting downstream of FgPacC.

To gain further insight into function of FgPacC in regulating histone acetylation during Fg infection, we performed genome-wide ChIP-seq to profile the chromatin landscape of H2BK11ac and H3K18ac in the wild-type PH-1 and the mutant ΔFgPacC inoculated in wheat heads at 120 hpi, and found that the accumulation of H2BK11ac and H3K18ac signals was globally more pronounced in ΔFgPacC than those in wild-type PH-1 (Figure 6B, C). In addition, both H2BK11ac and H3K18ac were predominately deposited around 5′ region of genes in Fg (Figure 6B, C). These results reveal that FgPacC inhibited histone acetylation during Fg infection. Next, we compared the H2BK11ac and H3K18ac signals at the iron uptake genes in ΔFgPacC and wild-type PH-1. As shown in Figure 6D, all of the 21 iron uptake genes displayed significantly increased
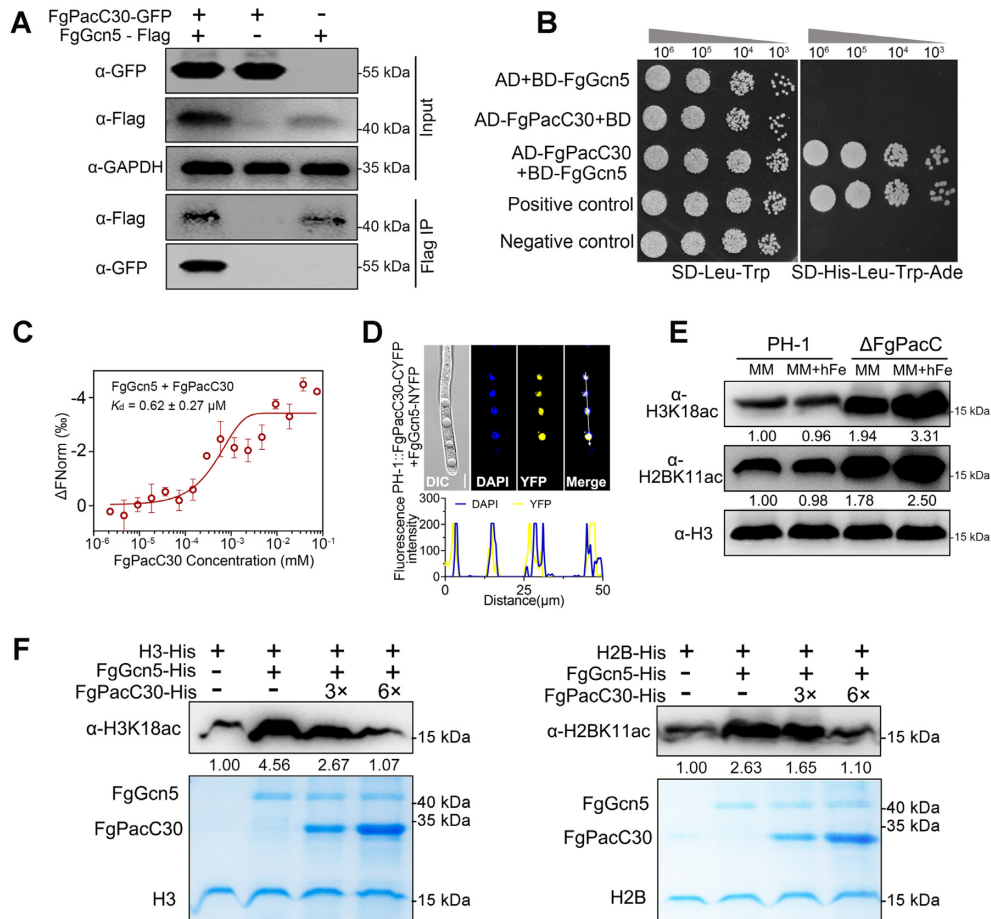
Figure 5. FgPacC30 binds to FgGcn5 and downregulates histone acetylation at H2BK11 and H3K18. (**A**) The association of FgPacC30 with FgGcn5 was verified via *in vivo* co-IP assay. Total proteins for each sample were extracted from each strain expressing FgPacC30-GFP with or without FgGcn5-Flag. The immune complexes were pulled down using anti-Flag agarose beads and immunoblotted with an anti-GFP and an anti-Flag antibody. GAPDH used as the loading control. (**B**) FgPacC30 interacted with FgGcn5 in Y2H assay. Serial dilutions of the yeast cells were plated on synthetic defined (SD) medium lacking leucine (L), tryptophan (T), histidine (H), and adenine (A) (SD-L-T-H-A). The yeast strain containing pGBKT7-53 and pGADT7 was used as a positive control, whereas that containing pGBKT7-Lam and pGADT7 was used as a negative control. (**C**) Microscale thermophoresis (MST) assays showed the binding of FgPacC30 with FgGcn5. The dissociation curve was fit to the data to calculate the K_d values. Data are presented as the mean ± standard deviation from three repeated experiments. (**D**) FgPacC30 interacted with FgGcn5 in the nucleus in bimolecular fluorescence complementation (BiFC) assay. The nuclear localization was confirmed by simultaneous nuclear staining with 4′-6-diamidino-2-phenylinodle (DAPI). Bar: 10 μm (upper panel). Colocalization of proteins was analyzed by line-scan graph analysis. The white arrow indicates the analyzed area. y axis: the intensity of YFP and DAPI signals quantified with ImageJ; x axis: the distance (μm) (lower panel). (**E**) FgPacC inhibited FgGcn5-mediated histone acetylation in Fg. Effect of FgPacC deletion on H3K18ac and H2BK11ac levels was determined by western blotting using anti-H3K18ac and anti-H2BK11ac antibodies. H3 protein was used as the loading control. The intensity of H3K18ac or H2BK11ac band from the wild-type PH-1 grown in MM was set as 1.00; and the relative intensity of H3K18ac or H2BK11 band from each treatment was quantified with ImageJ. (**F**) *In vitro* assay evaluating the inhibition of FgPacC30 against the HAT activity of FgGcn5 on H2BK11 and H3K18. Purified H3- or H2B-6 × His was incubated with FgGcn5-6 × His in HAT buffer in the absence or presence of FgPacC30 at different molar ratios (3 × or 6 × FgPacC30-His in relative to FgGcn5). The relative intensity of H3K18ac (left upper panel) or H2BK11 (right upper panel) band of each reaction was quantified with ImageJ. The band from the control reaction (only H3- or H2B-6 × His in HAT buffer) was set as 1.00. Protein loading control is shown by coomassie blue staining (left and right lower panels).

enrichments of H2BK11ac and H3K18ac in ΔFgPacC as compared to those of the wild type. These results support the model that FgPacC represses iron uptake genes expression during Fg infection through its inhibition of FgGcn5-mediated histone acetylation.

Ser137 of FgPacC30 determines its binding to FgGcn5

Zinc-fingers (ZnFs) are known as specific modules for protein-protein and protein-DNA interaction (70). Domain analysis indicates that FgPacC contains three C2H2-type zinc finger domains (ZnF1, ZnF2 and ZnF3) in the

N-terminal of FgPacC protein (Figure 7A). Y2H assays showed that the ZnF3 domain is necessary for interaction of FgPacC30 with FgGcn5 (Figure 7B). Next, we tried to define the fragment within the ZnF3 domain that is required for the interaction of FgPacC30 with FgGcn5. Based on the sequence of ZnF3 domain from different PacC homologues in *Pezizomycotina*, we identified a highly conserved fragment ZnF3 (133–143) corresponding to amino acid residues 133–143 of FgPacC (Figure 7D). Previous studies in yeast have shown that Gcn5 can target the sequences with an S-x-K-K/R-P motif (71). Notably, this putative Gcn5-binding motif (SFKRP, amino acid residues
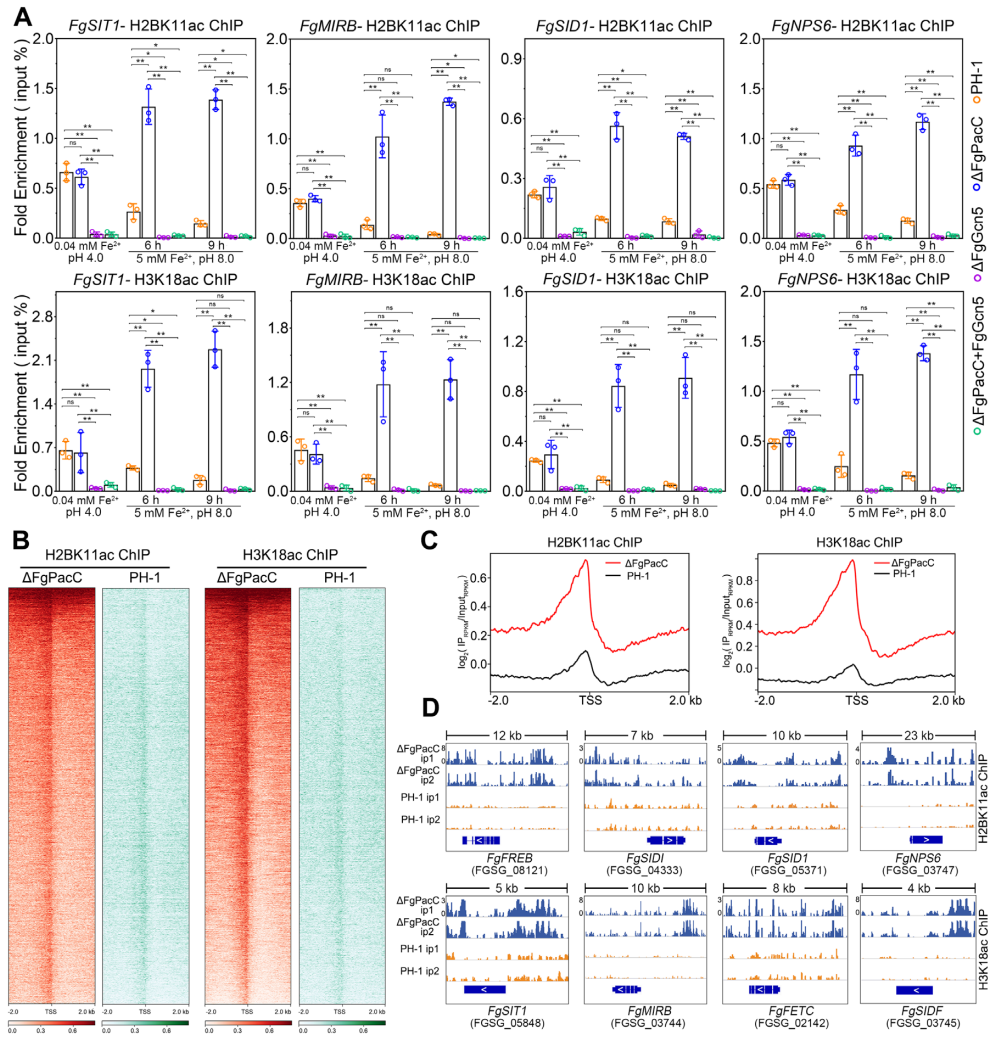
Figure 6. FgPacC30 inhibits FgGcn5-mediated histone acetylation during fungal infection. (**A**) ChIP-qPCR assays showed the H3K18ac and H2BK11ac deposition at the promoters of iron uptake genes, *FgNPS6*, *FgSID1*, *FgSIT1*, and *FgMIRB* in the wild-type PH-1, ΔFgPacC, ΔFgGcn5, and the double deletion mutant (ΔFgPacC + FgGcn5). Each strain was cultured in minimal medium (MM) under acidic and low-iron (0.04 mM Fe^{2+}, pH 4.0) conditions, and then subsequently incubated in MM under alkaline and high-iron (5 mM Fe^{2+}, pH 8.0) conditions for 6 h and 9 h. ChIP- and input-DNA samples were quantified by quantitative PCR assays. Data are presented as the mean ± standard deviation from three biological replicates. Statistical significance was determined using one-way ANOVA followed by Fisher's LSD test (ns: not significant, *$P < 0.05$, **$P < 0.01$). (**B**) Accumulation of H2BK11ac and H3K18ac were globally enhanced in ΔFgPacC as compared to those in the wild-type PH-1 inoculated on wheat heads at 120 hpi. Heatmaps showing the H2BK11ac and H3K18ac signals around the TSS (Transcription Start Site) of all tested genes in PH-1 and ΔFgPacC. The H2BK11ac and H3K18ac signals along TSS from –2 to + 2 kb are shown. (**C**) Profiles of global H2BK11ac and H3K18ac signals around TSS in PH-1 and ΔFgPacC. The ChIP signals were calculated as $\log_2(IP_{RPKM}/Input_{RPKM})$ for each 10 bp. (**D**) Representative examples of iron uptake genes showing enhanced enrichment of H2BK11ac or H3K18ac in the mutant ΔFgPacC than those in the wild-type PH-1. ChIP-seq data from two biological replicates (ip1 and ip2) were shown in the figure for ΔFgPacC and the wild-type PH-1 in the IGV (Integrative Genomics Viewer) browser. The ChIP signals were calculated as $\log_2(IP_{RPKM}/Input_{RPKM})$ for each 10 bp. Blue boxes with white arrows represent the open reading frames of iron uptake genes.

137–141) is localized in the ZnF3 (133–143) fragment of FgPacC30. Therefore, we proposed that SFKRP motif might mediate the FgPacC30-FgGcn5 interaction. To verify this hypothesis, we synthesized the ZnF3 (133–143) peptide and performed *in vitro* MST assays. As shown in Figure 7C, we observed a strong binding affinity of ZnF3 (133–143) with FgGcn5, indicating that this SFKRP-containing region is sufficient for FgGcn5-FgPacC30 interaction. Moreover, Y2H assays showed that the truncated FgPacC30$^{\Delta SFKRP}$ was unable to interact with Fg-Gcn5 (Figure 7B). To further test whether SFKRP motif is necessary for FgPacC30 function, we complemented

ΔFgPacC with a mutated FgPacC30$^{\Delta SFKRP}$. The resulting strain ΔFgPacC::FgPacC30$^{\Delta SFKRP}$ exhibited ∼51% inhibition of mycelial growth, but ΔFgPacC::FgPacC30 showed no inhibition by high-iron stress at pH 8.0 condition (Figure 7E), indicating that FgPacC30$^{\Delta SFKRP}$ was unable to restore the defect of ΔFgPacC in the high-iron stress tolerance under alkaline condition. Taken together, these results suggest that the SFKRP motif is essential for the interaction of Fg-PacC30 with FgGcn5.

Given that the ZnF domains may function as DNA-binding motifs that regulate genes expression, and ZnF3 (133–143) of FgPacC30 directly interacts with FgGcn5,
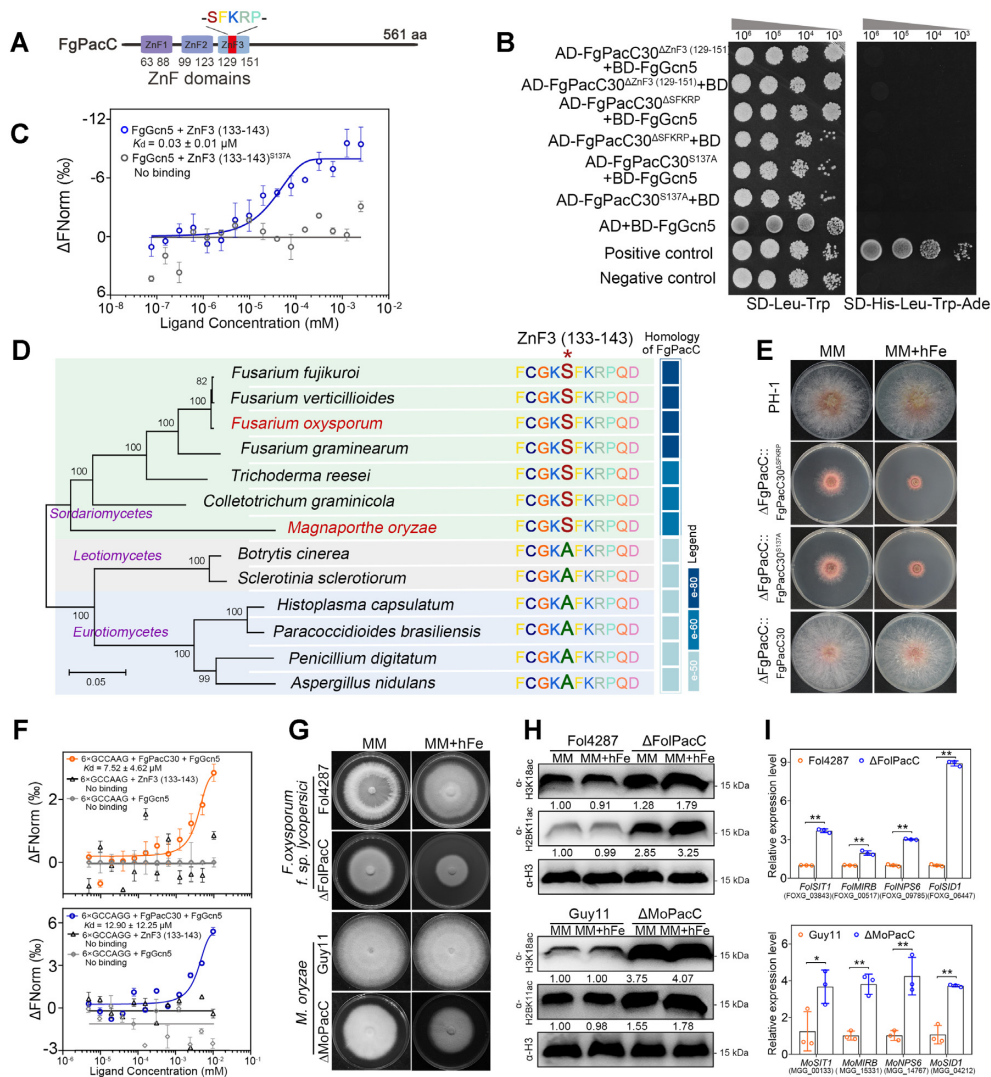
Figure 7. Ser137 of FgPacC30 is required for its interaction with FgGcn5. (**A**) Schematic view of the typical C_2H_2-type zinc fingers domain ZnF3 containing a SFKRP motif in the N-terminal of FgPacC. (**B**) Fine mapping of the FgGcn5-binding region in FgPacC30. Y2H assay revealed that a S137A substitution within the SFKRP motif led to disassociation of FgPacC30 with FgGcn5. Serial dilutions of the yeast cells were plated on synthetic defined (SD) medium lacking leucine (L), tryptophan (T), histidine (H), and adenine (A) (SD-L-T-H-A). The yeast strain bearing pGBKT7-53 and pGADT7 was used as a positive control, whereas the strain containing pGBKT7-Lam and pGADT7 was used as a negative control. (**C**) S137 of FgPacC30 is the key residue required for the interaction with FgGcn5. Microscale thermophoresis (MST) assays showed FgGcn5 bound with ZnF3 (133–143) (FCGKSFKRPQD) but not with the mutated ZnF3(133–143)^{S137A} (FCGKAFKRPQD) of FgPac30. The dissociation curve was fit to the data to calculate the K_d values. Data are presented as the mean ± standard deviation from three repeated experiments. (**D**) S137 of FgPacC30 is conserved in *Sordariomycetes*, while a S137A substitution was widespread in *Leotiomycetes* and *Eurotiomycetes* fungi. The phylogenetic tree was constructed based on the amino acid sequences of RPB2 from 13 *Pezizomycotina* fungal species with Mega 5.0 using the neighbor-joining method. (**E**) Determination of sensitivity of the wild-type PH-1, ΔFgPacC::FgPacC30^{ΔSFKRP}, ΔFgPacC::FgPacC30^{S137A}, and ΔFgPacC::FgPacC30 to high-iron stress at pH 8.0. (**F**) Microscale thermophoresis (MST) assay showed that the ZnF3 (133–143) domain of FgPac30 was unable to bind to the *cis*-element GCCAR(R = A/G)G, and FgPac30 could bind with its *cis*-element 6 × GCCAR(R = A/G)G in the presence of FgGcn5. Data are presented as the mean ± standard deviation from three repeated experiments. (**G**) Deletion of FgPacC homologues in *Sordariomycetes* fungi, *F. oxysporum* and *M. oryzae* led to increased sensitivity to high-iron stress. (**H**) Elevated H2BK11ac and H3K18ac levels in the mutants ΔFolPacC and ΔMoPacC as compared to these in their wild type strains Fol4287 and Guy11, respectively. (**I**) Enhanced expression of iron uptake genes in the mutants ΔFolPacC, and ΔMoPacC at pH 8.0. Expression of iron uptake genes in *F. oxysporum* and *M. oryzae PACC* mutants was evaluated by RT-qPCR using *FolACTIN* gene and *MoACTIN* as the internal control, respectively. Expression of iron uptake genes in *F. oxysporum* wild-type strain Fol4287 or *M. oryzae* wild-type Guy11 was set as 1.0. Data are presented as the mean ± standard deviation from three biological replicates. Statistical significance compared to wild-type strain Fol4287 or Guy11 was determined using Student's *t*-test (ns: not significant, * $P < 0.05$, ** $P < 0.01$).

we next examined whether interaction of FgGcn5 with the ZnF3 domain of FgPacC30 disrupts the binding of FgPac30 with its target DNA element $6 \times$ GC-CAR(R = A/G)G. MST assays showed that the ZnF3 (133–143) peptide was unable to bind to the *cis*-element $6 \times$ GC-CAR(R = A/G)G (Figure 7F), indicating the ZnF3 domain of FgPacC30 is not a functional domain responsible for the binding of FgPacC30 with its *cis*-element. In addition, the binding affinity of FgPacC30 with $6 \times$ GC-CAR(R = A/G)G showed no obvious change in the absence or presence of FgGcn5 (Figure 4E and 7F, respectively), indicating that the interaction of FgGcn5 with FgPacC30 did not interfere with the binding of FgPacC30 to its *cis*-element GCCAR(R = A/G)G at the promoters of iron uptake genes.

To investigate the evolutionary trajectories of SFKRP motif in PacC, we searched for PacC homologues in 13 *Pezizomycotina* fungal species. Sequence alignment using ClustalW showed that the SFKRP motif in different *Sordariomycetes* PacC homologues is entirely conserved; however, a S137A substitution was widely present in *Leotiomycetes* and *Eurotiomycetes* (Figure 7D). To determine whether this substitution would affect the FgPacC30-FgGcn5 interaction, we generated a mutated FgPacC30^{S137A}, where the S137 residue was substituted with A, and carried out Y2H assays. The Y2H assays showed that the mutated FgPacC30^{S137A} was no longer able to interact with FgGcn5 (Figure 7B). Furthermore, we synthesized a mutated ZnF3 (133–143) peptide containing a S137A substitution (named ZnF3 (133–143)^{S137A}). By using MST, we found that the ZnF3 (133–143)^{S137A} peptide was unable to bind to FgGcn5 (Figure 7C), demonstrating that S137 residue plays a critical role in FgPacC30-FgGcn5 interaction. Moreover, we complemented ΔFgPacC with a mutated FgPacC30^{S137A} and the resulting strain ΔFgPacC::FgPacC30^{S137A} showed ∼52% inhibition of mycelial growth by high-iron stress at pH 8.0 condition (Figure 7E), indicating that FgPacC30^{S137A} failed to restore the defects of ΔFgPacC in high-iron stress tolerance under alkaline condition. Taken together, these results indicate that S137 residue is conserved in *Sordariomycetes* PacC homologues and determines the FgGcn5-FgPacC30 interaction.

Since the key S137 residue is widespread in *Sordariomycetes* PacC homologues, we further evaluated whether this PacC-mediated epigenetic regulatory mechanism of iron homeostasis is evolutionary conserved in *Sordariomycetes*. To do this, we knocked out FgPacC homologues in *Sordariomycetes* fungal species, *F. oxysporum* and *M. oryzae*. Phenotypic characterizations revealed that ΔFolPacC and ΔMoPacC mutants displayed increased sensitivity to high-iron stress in comparison with the wild type at alkaline pH condition (Figure 7G). Consistently, as shown in Figure 7H, the H2BK11ac and H3K18ac levels were elevated in ΔFolPacC and ΔMoPacC. RT-qPCR assays showed that the key iron uptake genes were also significantly upregulated in ΔFolPacC and ΔMoPacC (Figure 7I). Taken together, these findings suggest that FgPacC is functionally conserved in *Sordariomycetes* to regulate high-iron stress response.

FgPacC30 is phosphorylated at Ser2 upon high-iron stress

Next, we aimed to investigate how FgPacC30 senses extracellular high-iron stress. In eukaryotes, transcription factors are frequently phosphorylated or dephosphorylated in response to extracellular signals (72) and previous data shows *A. nidulans* PacC can be heavily phosphorylated, presumably a signal for proteolysis (64). Therefore, we first tested whether FgPacC30 is phosphorylated in response to high-iron stress. Phos-tag assays showed that the phosphorylated isoforms of FgPacC30 increased under high-iron stress (Figure 8A), indicating that the phosphorylation of FgPacC30 was induced in response to high-iron stress. Moreover, the phosphoproteome assay revealed that the serine residue at 2 site (Ser2) of N terminus in FgPacC might be subject to phosphorylation (Supplementary Figure S12). In agreement with the evolutionary conserved function of PacC in high-iron adaption, the site Ser2 is evolutionary conserved in PacC homologues from *Sordariomycetes* fungi (Figure 8B). To explore the roles of FgPacC phosphorylation in high-iron stress response, we constructed strains containing phosphor-inactive or phosphorymimetic FgPacC30. Briefly, the predicted phosphorylation residue S2 was replaced by alanine (A) to mimic dephosphorylation status, or aspartic acid (D) to mimic phosphorylated condition, respectively (Figure 8B). The mutated FgPacC30^{S2A}-Flag and FgPacC30^{S2D}-Flag alleles were then transformed into the mutant strain ΔFgPacC, and the resulting strains were designated as ΔFgPacC::FgPacC30^{S2A}-Flag and ΔFgPacC::FgPacC30^{S2D}-Flag, respectively. Phos-tag assays showed that FgPacC30 was normally phosphorylated in ΔFgPacC, but FgPacC30^{S2A} could not be phosphorylated in the strain ΔFgPacC::FgPacC30^{S2A}-Flag under high-iron stress (Figure 8C). Phenotypic analysis revealed that similar to ΔFgPacC, ΔFgPacC::FgPacC30^{S2A}-Flag displayed increased sensitivity to high-iron stress at alkaline pH conditions as compared with wild-type PH-1 (Figure 8D). In contrast, ΔFgPacC::FgPacC30^{S2D}-Flag showed significant growth defects, and exhibited enhanced tolerance to high-iron stress than wild-type PH-1 at alkaline pH conditions (Figure 8D). Consistently, the expression of key iron uptake genes, *FgNPS6*, *FgSID1*, *FgSIT1* and *FgMIRB*, were significantly elevated in ΔFgPacC::FgPacC30^{S2A}-Flag, but reduced in ΔFgPacC::FgPacC30^{S2D}-Flag (Figure 8E), indicating that the phosphorylation at Ser2 of FgPacC30 is required for the repression of iron uptake genes.

To test whether the phosphorylation of FgPacC30 could impact FgGcn5-mediated histone acetylation, we determined the H3K18ac and H2BK11ac levels in FgPacC phosphor-inactive or phosphorymimetic strains. The global H3K18ac and H2BK11ac levels were markedly enhanced in ΔFgPacC::FgPacC30^{S2A}-Flag, but reduced in ΔFgPacC::FgPacC30^{S2D}-Flag as shown by western blot (Figure 8F). Moreover, ChIP-qPCR assays showed that H3K18ac and H2BK11ac enrichments at these iron uptake genes were significantly increased in ΔFgPacC::FgPacC30^{S2A}-Flag, but decreased in ΔFgPacC::FgPacC30^{S2D}-Flag (Figure 8G). Taken together, these data indicate that phosphorylation at Ser2
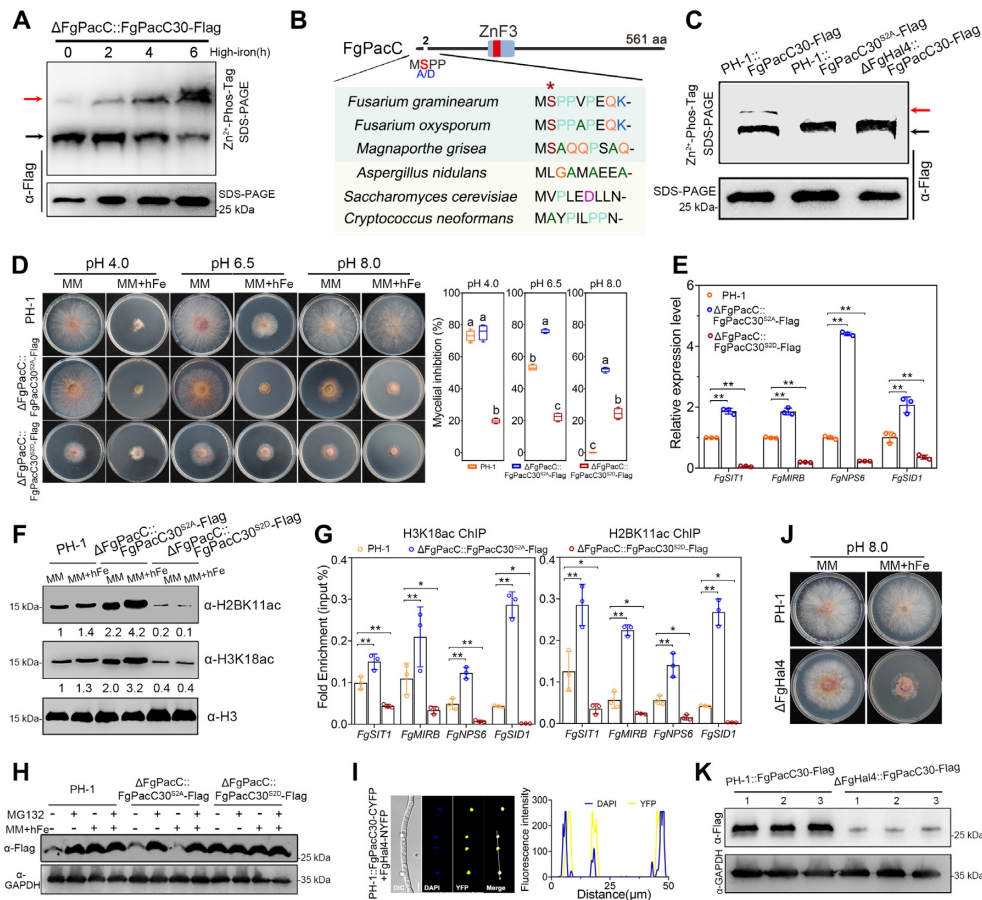
Figure 8. FgHal4 promotes the phosphorylation of FgPacC30 and protects FgPacC30 against 26S proteasome-dependent degradation under high-iron condition. (**A**) Phos-tag assays showed that FgPacC30 was phosphorylated in response to extracellular high-iron stress. The dephosphorylated and phosphorylated FgPacC30 are indicated with black and red arrows, respectively (upper panel). Each protein sample was also subjected to normal SDS-PAGE followed by immunoblotting with the anti-Flag antibody as the loading control (lower panel). (**B**) Sketch map of the phosphorylated residue in FgPacC30 (upper panel). The phosphorylation site Ser2 is conserved in PacC homologues from *Sordariomycetes* fungi (*Fusarium graminearum*, *Fusarium oxysporum* and *Magnaporthe oryzae*), but not in *Saccharomyces cerevisiae*, *Aspergillus nidulans* and *Cryptococcus neoformans*. Sequence alignment was performed by ClustalW (lower panel). (**C**) The phosphorylation status of FgPacC30 or FgPacC30^{S2A} in wild-type PH-1 or the mutant ΔFgHal4 background was determined by Phos-tag assays. The dephosphorylated and phosphorylated FgPacC30 or FgPacC30^{S2A} are indicated with black and red arrows, respectively (upper panel). Proteins extracted from each strain were also subjected to normal SDS-PAGE followed by immunoblotting with an anti-Flag antibody as loading controls (lower panel). (**D**) Determination of sensitivity of the wild-type PH-1, ΔFgPacC::FgPacC30^{S2A}-Flag, and ΔFgPacC::FgPacC30^{S2D}-Flag to high-iron stress at different pH (left panel). Mycelial inhibition by the high-iron stress relative to each untreated control was calculated for each strain at pH 4.0, 6.5 and 8.0, respectively (right panel). Data are presented as the mean ± standard deviation from four biological replicates. Different letters (a, b, and c) represent significant differences statistically according to the one-way ANOVA followed by Fisher's LSD test ($P < 0.05$). (**E**) Comparisons of expression of iron uptake genes among the wild-type PH-1, ΔFgPacC::FgPacC30^{S2A}-Flag and ΔFgPacC::FgPacC30^{S2D}-Flag were evaluated by RT-qPCR using *FgACTIN* gene as the internal control. Expression of each iron uptake gene in the wild-type PH-1 was set as 1.0. Data are presented as the mean ± standard deviation from three biological replicates. Statistical significance was determined using one-way ANOVA followed by Fisher's LSD test (ns: not significant, $** P < 0.01$). (**F**) FgPacC phosphorylation negatively regulated histone acetylation at H3K18 and H2BK11 in Fg. H3 of each sample was used as a loading control. (**G**) ChIP-qPCR assays showed that FgPacC phosphorylation inhibited the H3K18ac and H2BK11ac deposition at the promoters of iron uptake genes. ChIP- and input-DNA samples were quantified by quantitative PCR assays. Data are presented as the mean ± standard deviation from three biological replicates. Statistical significance was determined using one-way ANOVA followed by Fisher's LSD test ($*P < 0.05$, $** P < 0.01$). (**H**) The 26S proteasome inhibitor MG132 inhibited the degradation of unphosphorylated FgPacC30 under high-iron stress condition. The accumulation of FgPacC30-Flag, FgPacC30^{S2A}-Flag or FgPacC30^{S2D}-Flag was determined by immunoblot analysis after treatment for 6 hours with or without 5 mM Fe^{2+} or 200 μM MG132. (**I**) Bimolecular fluorescence complementation (BiFC) assay showed that FgPacC30 interacted with FgHal4 in the nucleus. The nuclear localization was confirmed by simultaneous nuclear staining with 4′-6-diamidino-2-phenylinodle (DAPI). Bar: 10 μm. White arrows highlight areas analyzed by line-scan graph analysis. y axis: the intensity of YFP and DAPI signals quantified by ImageJ; x axis: the distance (μm) (right panel). (**J**) ΔFgHal4 showed increased sensitivity to high-iron stress. A five-mm mycelial plug of each strain was incubated for three days on minimal medium (MM) supplement with or without 5 mM Fe^{2+} at pH 8.0. (**K**) FgHal4 was required for FgPacC30 accumulation upon high-iron stress. The amounts of FgPacC30-Flag under high-iron treatment were detected by western blot using anti-Flag antibody. 1–3 represents three independent transformants containing FgPacC30-Flag in the background strain of wild-type PH-1 or the mutant ΔFgHal4. FgGAPDH used as the loading control.

of FgPacC is required for epigenetically repressing the expression of iron uptake genes.

Phosphorylation at Ser2 protects FgPacC30 against proteasome-dependent degradation

Signal-dependent degradation of transcription factors through ubiquitin-26S proteasome system represents a crucial mechanism of transcriptional regulation (73,74). From the affinity capture assays, we found that FgPacC30 might interact with the ubiquitin-26S proteasome (Supplementary Table S2), suggesting that FgPacC30 may be subjected to 26S proteasome mediated degradation, possibly in a manner analogous to PacC processing in *A. nidulans* (64). Then, we examined the protein abundance of FgPacC30 in the strain ΔFgPacC::FgPacC30-Flag via immunoblot analysis using anti-Flag antibody. The results showed that the protein abundance of FgPacC30 was substantially increased with high-iron treatment (Figure 8A, H). Moreover, this increase in FgPacC30 protein abundance could also be induced by the 26S proteasome inhibitor [z-Leu-Leu-Leu-CHO (MG132)] even without high-iron treatment (Figure 8H). These results suggested that high-iron stress likely inhibits the 26S proteasome-dependent degradation of FgPacC30, leading to the FgPacC30 accumulation.

To dissect the biological significance of FgPacC30 phosphorylation on protein stability, we further examined the protein levels of phospho-inactive FgPacC30^{S2A} and phosphorymimetic FgPacC30^{S2D} in the ΔFgPacC::FgPacC30^{S2A}-Flag and ΔFgPacC::FgPacC30^{S2D}-Flag. The results showed that FgPacC30^{S2A} protein accumulated at a low level even under high-iron conditions, while MG132 treatment could significantly increase the protein abundance of FgPacC30^{S2A} (Figure 8H). By contrast, FgPacC30^{S2D} showed significant protein accumulation even without high-iron treatment (Figure 8H). Therefore, these results support the model that high-iron stress mediated the phosphorylation of FgPacC30 at Ser2, thus protecting FgPacC30 against protein degradation mediated by 26S proteasome system.

FgHal4 is highly induced by high-iron stress and mediates the phosphorylation of FgPacC30, thus preventing its degradation

Next, we tried to identify the potential protein kinase that is required for the phosphorylation of FgPacC30. From the affinity capture assay, we identified a Ser/Thr protein kinase FgHal4 might interact with FgPacC30 (Supplementary Table S2). Furthermore, co-IP and Y2H assays verified the association of FgPacC30 with FgHal4 (Supplementary Figure S13A, B). BiFC assay also showed that FgHal4 could interact with FgPacC30 in the nucleus (Figure 8I). *In planta* RT-qPCR assays indicated that *FgHAL4* expression was notably induced at 48–120 hpi (Supplementary Figure S13C). Interestingly, under *in vitro* conditions, we found that *FgHAL4* was highly induced at high-iron condition, but not at alkaline pH condition (Supplementary Figure S13D). Furthermore, we generated the deletion mutant of FgHal4 and found that ΔFgHal4 showed similar defects with ΔFgPacC in high-iron resistance under alkaline condition (Figure 8J). These results suggest that FgHal4 is likely

highly induced by host-derived high-iron signal and associated with FgPacC30 to regulate high-iron stress response during infection.

Next, we performed a Phos-tag assay to verify the function of FgHal4 in regulating FgPacC phosphorylation. The results showed that the phosphorylation of FgPacC30 was abolished in the mutant ΔFgHal4 under high-iron stress (Figure 8C). Furthermore, the increased FgPacC30 protein accumulation induced by high-iron stress was notably attenuated in ΔFgHal4 in comparison to that in wild-type PH-1 (Figure 8K). These results indicate that FgHal4 promotes the phosphorylation of FgPacC30 upon high-iron stress and protects its degradation via 26S proteasome system.

DISCUSSION

Balance of intracellular iron levels is necessary for every organism. In plant-pathogen interactions, host plants evolve multiple strategies to perturb iron homeostasis of pathogens, thus restricting their infection (5,7). Previous studies have shown that Poaceae plants, such as wheat and maize, can locally accumulate iron to wield against fungal pathogens (5,10,11). Consistently, this study shows that wheat plants can locally increase iron levels during Fg infection, leading to high-iron stress against the pathogen infectious growth. Moreover, this study found that FgPacC serves as a major regulator for iron stress response during Fg infection. PacC was known as a pH regulatory factor and plays an pivotal role in secondary metabolism in pathogenetic fungi, including Fg, *Fusarium fujikuroi*, *Ganoderma lucidum*, *Beauveria bassiana*, and *Aspergillus* spp. (75–81). Here we showed that FgPacC is a key regulator for alkaline pH response. More importantly, we demonstrated that during infection, FgPacC undergoes a proteolytic cleavage into the functional isoform FgPacC30, which subsequently binds to a GCCAR(R = A/G)G motif at the promoters of genes involved in iron uptake and inhibits their expression. This FgPacC-dependent adaption to high-iron stress may enable the infectious growth and survival of Fg within the host plant. Therefore, we present a previously unreported regulatory mechanism of high-iron stress responses mediated by FgPacC during fungal infection, providing novel insights into transcriptional regulation of iron homeostasis in eukaryotes.

Acetylation or deacetylation of histone proteins acts as a critical epigenetic switch to turn on or off eukaryotic genes (18). Histone mediated by HATs often represents an active chromatin configuration that is associated with transcriptional activation; whereas histone deacetylation catalyzed by HDACs induces a repressed chromatin state and transcriptional repression (82,83). The SAGA complex, containing the Gcn5 HAT, is conserved in most eukaryotes, and functions as a transcriptional coactivator (84). Recently, the functions of the SAGA complex have been well-characterized in plants, animal systems, as well as in some filamentous fungi (84–86). In *S. cerevisiae*, the DNA-binding activators (such as Gcn4 and Swi5) recruit SAGA complex to the promoters of its target genes to generate a localized domain of modified histones, leading to the transcriptional activation (87,88). Increasing evidence in-

dicates that SAGA-mediated histone acetylation dynamics is tightly linked with iron homeostasis in eukaryotic cells. In *A. thaliana*, Gcn5-mediated H3K9ac and H3K14ac of FDR3 contribute to iron uptake (89). In mammalian cells, histone deacetylase 3 is epigenetically involved in suppression of hepcidin expression, thus governing systemic iron homeostasis (90). More recently, in the human fungal pathogen *C. albicans*, the interplay of transcriptional regulators Hap43, Sef1 and trimeric HAP complex regulates the H3K9ac levels at the promoters of iron homeostasis genes and fine-tunes their expression (91). Although it has been well documented that the SAGA complex controls gene transcription by modifying histone acetylation, the molecular mechanisms that tightly regulate the activity of SAGA complex remain largely unknown. In the present study, we demonstrate that the functional isoform of a fungal transcriptional factor FgPacC30 directly binds FgGcn5 to inhibit its HAT activity, leading to the downregulation of histone acetylation at H2BK11 and H3K18 at target genes; subsequently represses expression of iron uptake genes (Figure 9). To the best of our knowledge, this is the first report of an inhibitory mechanism for SAGA complex mediated by a transcription factor that enables the transcriptional repression of specific genes at an epigenetic level. Apart from regulation of iron uptake, FgGcn5 was reported to activate the expression of genes involved in fungal development, secondary metabolism and virulence (26,92). Based on previously published RNA-seq data, FgGcn5 could also repress the expression of virulence-related genes (such as *Fg-STE12*, *FgRLM1* and *FgMEC1*), and may play negative roles in regulating Fg virulence (92). In this study, we found that ΔFgGcn5 and ΔFgPacC + FgGcn5 displayed stronger defects in mycelial growth and virulence than ΔFgPacC. Therefore, it is likely that FgGcn5 plays both positively and negatively regulatory roles in fungal growth and virulence by acting downstream of FgPacC, and may be also independent of this factor partly.

During infection, many fungal pathogens can induce either a pH upshift or downshift in the surrounding host tissues. In a number of fruit fungal pathogens, such as *Colletotrichum spp*. and *Alternaria alternata,* the fungi alkalinize the host tissues by release of ammonia and thus drive fungal pathogenesis (54,93). Whereas, the root-infecting fungus, *Fusarium oxysporum*, is able to trigger host alkalinization by secreting a functional homologue of rapid alkalinizing factor (RALF) to increase its infectious potential and suppress host immunity (53). In this study, we found that Fg infection triggered an increase of almost 3 units of the pH in wheat tissues during 48–96 hpi, resulting in alkalinization of the host plant. However, the underlying mechanism of how Fg provokes host alkalinization remains unclear.

In response to ambient pH upshifts, fungi evolve a conserved Pal/Rim signaling pathway, which was first described in ascomycete fungi *A. nidulans* and *S. cerevisiae* (94). In *A. nidulans*, the transmembrane protein PalH senses alkaline pH signal and mediates ubiquitination and phosphorylation of PalF, leading to endocytosis of the receptor complex and recruitment of the endosomal sorting complexes required for transport (ESCRT) to the plasma membrane (94). This results in the activation and processing of the zinc finger transcription factor PacC through the PalA-PalB-PalC involved proteasome. The truncated PacC is subsequently translocated into nucleus and induces the activation of alkaline-expressed genes and repression of acid-expressed genes (63,94). Similar mechanisms involving the PacC signaling pathway have also been reported in fungal pathogens, such as *F. oxysporum*, *Yarrowia lipolytica* and *C. neoformans* (95–97), indicating the pH signaling system is widely conserved throughout the fungi kingdom. In this study, we found that Fg-provoked plant alkalinization on wheat tissues triggers the proteolytic cleavage of Fg-PacC into the functional isoform FgPacC30. The FgPac30 is translocated into the nucleus and binds to FgGcn5 to inhibit its HAT activity, thus transcriptionally downregulating expression of the iron uptake genes, subsequently promoting Fg infection. These results suggest that Fg-induced host alkalinization confers the adaption of the fungus to host-derived high-iron stress during infection. While Gcn5 is well known as its roles in targeting histones, it also acetylates non-histone substrates to regulate diverse aspects of cell physiology (98). Since FgGcn5 acetylates histones in the nucleus, the processing and nuclear translocation of FgPacC seem to be required for its inhibitory function in FgGcn5-dependent histone acetylation. However, it currently remains unclear whether the full length of FgPacC associates with FgGcn5 in the cytoplasm and inhibits the FgGcn5-mediated acetylation of non-histone proteins.

Phosphorylation of transcription factors mediated by various protein kinases is an important mechanism for eukaryotic cells to regulate their DNA binding ability and protein accumulation in response to the environmental stimuli (72,99). Recently, this phosphorylation-dependent modulation of transcription factor activity was also reported to be employed by cells to sense the external iron signals. In *A. thaliana*, the phosphorylated transcription factor URI was found to accumulate during iron-deficiency, and consequently driving the iron uptake (100). FIT, a key transcription factor responsible for regulating iron uptake in plants, was also found to be deactivated through Tyr phosphorylation (101). In the yeast *S. cerevisiae*, the Hog1 kinase negatively regulates iron uptake by phosphorylating the low-iron sensing transcription factor Atf1 (102). Here, we found that the protein kinase FgHal4 is highly induced by host-derived high-iron stress although it remains unclear how the high-iron stress induces transcription of FgHal4. In addition, FgHal4 interacts with FgPacC30 and is responsible for the phosphorylation of FgPacC30. The phosphorylated FgPacC30 is subsequently able to avoid 26S proteasome-dependent degradation, leading to the protein accumulation (Figure 9). However, it is currently unclear whether the C-terminal cleavage and nuclear translocation of FgPacC occur prior to the high-iron induction of FgPacC phosphorylation.

Phylogenetic analysis showed that Ser2 is widely present in PacC homologues from *Sordariomycetes* but not from *S. cerevisiae* and *A. nidulans*. Consistently, the *S. cerevisiae* Hal4 was unable to sense the high-iron condition (Supplementary Figure S14). In addition to Ser2, we found that the S137 residue is also conserved in PacC homologues from *Sordariomycetes*, but the S137A substitution is widespread in *Leotiomycetes* and *Eurotiomycetes*. Based on the Y2H and MST results, we observed that the S137 of FgPacC30 is a key residue required for the interaction of FgPacC30
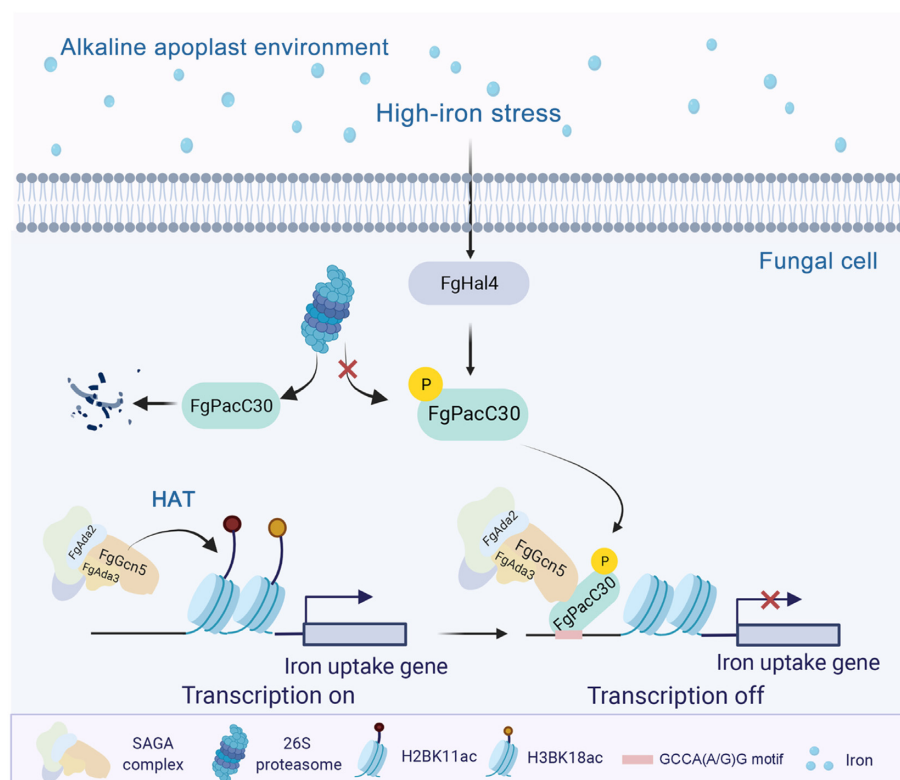
Figure 9. A proposed model for epigenetic regulation of iron uptake genes during Fg-wheat interactions. Fg infection induces plant alkalinization and high-iron stress in wheat tissues. At alkaline and high-iron host environment, the protein kinase FgHal4 is highly induced and promotes the phosphorylation of FgPacC30. The phosphorylated FgPacC30 is able to avoid the protein degradation via 26S proteasome pathway, leading to the protein accumulation. The accumulated FgPacC30 binds to FgGcn5 and inhibits its HAT activity, leading to deregulation of histone acetylation at H3K18 and H2BK11, and repression of iron uptake genes. Subsequently, Fg enhances adaption to host-derived high-iron stress during infection. Figure created using BioRender (http://biorender.com/).

with FgGcn5, and the S137A substitution blocks this interaction (Figure 7B, C). Consistently, deletion of FgPacC homologues in *Sordariomycetes* fungi, *F. oxysporum* and *M. oryzae*, also lead to deregulation of histone acetylation and iron uptake genes repression. Therefore, our findings indicate that PacC is functionally conserved and serves as a repressor for iron uptake in *Sordariomycetes* by inhibiting the HAT activity of Gcn5.

In conclusion, we report a fungal transcription factor Fg-PacC that can directly bind and inhibit the HAT activity of FgGcn5, subsequently enhances adaption of Fg to host-derived high-iron stress during infection. This effective epigenetic regulatory mechanism enables fungal pathogens to rapidly and precisely respond to dynamic host microenvironments.

DATA AVAILABILITY

Relevant data supporting the findings of this study are available in this article and its Supplementary Information files. Raw and processed data for RNA-seq, ChIP-seq are available in the GEO repository under the accession number GSE203093. The mass spectrometry proteomics data have been deposited to the ProteomeXchange Consortium (http://proteomecentral.proteomexchange.org) with the dataset identifier PXD029059. Source data are provided with this paper.

SUPPLEMENTARY DATA

Supplementary Data are available at NAR Online.

REFERENCES

1. Aisen,P., Enns,C. and Wessling-Resnick,M. (2001) Chemistry and biology of eukaryotic iron metabolism. *Int. J. Biochem. Cell Biol.*, **33**, 940–959.
2. Kobayashi,T. and Nishizawa,N.K. (2012) Iron uptake, translocation, and regulation in higher plants. *Annu. Rev. Plant Biol.*, **63**, 131–152.
3. Ehrensberger,K.M. and Bird,A.J. (2011) Hammering out details: regulating metal levels in eukaryotes. *Trends Biochem. Sci*, **36**, 524–531.
4. Cassat,J.E. and Skaar,E.P. (2013) Iron in infection and immunity. *Cell Host Microbe*, **13**, 509–519.
5. Verbon,E.H., Trapet,P.L., Stringlis,I.A., Kruijs,S., Bakker,P.A.H.M. and Pieterse,C.M.J. (2017) Iron and immunity. *Annu. Rev. Phytopathol.*, **55**, 355–375.
6. Ganz,T. and Nemeth,E. (2015) Iron homeostasis in host defence and inflammation. *Nat. Rev. Immunol.*, **15**, 500–510.
7. Expert,D., Enard,C. and Masclaux,C. (1996) The role of iron in plant host–pathogen interactions. *Trends Microbiol.*, **4**, 232–237.
8. Franza,T. and Expert,D. (2013) Role of iron homeostasis in the virulence of phytopathogenic bacteria: an 'a la carte' menu. *Mol. Plant Pathol.*, **14**, 429–438.
9. Lemanceau,P., Expert,D., Gaymard,F., Bakker,P.A.H.M. and Briat,J.F. (2009) Role of iron in plant-microbe interactions. *Adv Bot Res*, **51**, 491–549.
10. Aznar,A., Chen,N.W., Thomine,S. and Dellagi,A. (2015) Immunity to plant pathogens and iron homeostasis. *Plant Sci.*, **240**, 90–97.
11. Greenshields,D.L., Liu,G. and Wei,Y. (2007) Roles of iron in plant defence and fungal virulence. *Plant Signal Behav.*, **2**, 300–302.
12. Liu,G., Greenshields,D.L., Sammynaiken,R., Hirji,R.N., Selvaraj,G. and Wei,Y. (2007) Targeted alterations in iron homeostasis underlie plant defense responses. *J. Cell Sci.*, **120**, 596–605.
13. Ye,F., Albarouki,E., Lingam,B., Deising,H.B. and von Wiren,N. (2014) An adequate fe nutritional status of maize suppresses infection and biotrophic growth of *colletotrichumgraminicola*. *Physiol. Plant.*, **151**, 280–292.
14. Jenner,R.G. and Young,R.A. (2005) Insights into host responses against pathogens from transcriptional profiling. *Nat. Rev. Microbiol.*, **3**, 281–294.
15. van der Does,H.C. and Rep,M. (2017) Adaptation to the host environment by plant-pathogenic fungi. *Annu. Rev. Phytopathol.*, **55**, 427–450.
16. Gaston,K. and Jayaraman,P.S. (2003) Transcriptional repression in eukaryotes: repressors and repression mechanisms. *Cell. Mol. Life Sci.*, **60**, 721–741.
17. Jaenisch,R. and Bird,A. (2003) Epigenetic regulation of gene expression: how the genome integrates intrinsic and environmental signals. *Nat. Genet.*, **33**, 245–254.
18. Howe,L., Brown,C.E., Lechner,T. and Workman,J.L. (1999) Histone acetyltransferase complexes and their link to transcription. *Crit. Rev. Eukar. Gene*, **9**, 231–243.
19. Candau,R., Zhou,J.X., Allis,C.D. and Berger,S.L. (1997) Histone acetyltransferase activity and interaction with ADA2 are critical for GCN5 function in vivo. *EMBO J.*, **16**, 555–565.
20. Bonnet,J., Wang,C.Y., Baptista,T., Vincent,S.D., Hsiao,W.C., Stierle,M., Kao,C.F., Tora,L. and Devys,D. (2014) The SAGA coactivator complex acts on the whole transcribed genome and is required for RNA polymerase II transcription. *Genes Dev.*, **28**, 1999–2012.
21. Donczew,R., Warfield,L., Pacheco,D., Erijman,A. and Hahn,S. (2020) Two roles for the yeast transcription coactivator SAGA and a set of genes redundantly regulated by TFIID and SAGA. *Elife*, **9**, e50109.
22. Chang,P., Fan,X. and Chen,J. (2015) Function and subcellular localization of gcn5, a histone acetyltransferase in *Candida albicans*. *Fungal Genet. Biol.*, **81**, 132–141.
23. O'Meara,T.R., Hay,C., Price,M.S., Giles,S. and Alspaugh,J.A. (2010) *Cryptococcus neoformans* histone acetyltransferase gcn5 regulates fungal adaptation to the host. *Eukaryot Cell*, **9**, 1193–1202.
24. Gonzalez-Prieto,J.M., Rosas-Quijano,R., Dominguez,A. and Ruiz-Herrera,J. (2014) The umgcn5 gene encoding histone acetyltransferase from *ustilagomaydis* is involved in dimorphism and virulence. *Fungal Genet. Biol.*, **71**, 86–95.
25. Rosler,S.M., Kramer,K., Finkemeier,I., Humpf,H.U. and Tudzynski,B. (2016) The SAGA complex in the rice pathogen *Fusarium fujikuroi*: structure and functional characterization. *Mol. Microbiol.*, **102**, 951–974.
26. Chen,Y., Wang,J., Yang,N., Wen,Z.Y., Sun,X.P., Chai,Y.R. and Ma,Z.H. (2018) Wheat microbiome bacteria can reduce virulence of a plant pathogenic fungus by altering histone acetylation. *Nat. Commun.*, **9**, 3429.
27. Nutzmann,H.W., Reyes-Dominguez,Y., Scherlach,K., Schroeckh,V., Horn,F., Gacek,A., Schumann,J., Hertweck,C., Strauss,J. and Brakhage,A.A. (2011) Bacteria-induced natural product formation in the fungus *Aspergillus nidulans* requires Saga/Ada-mediated histone acetylation. *Proc. Natl. Acad. Sci. U.S.A.*, **108**, 14282–14287.
28. Bok,J.W., Soukup,A.A., Chadwick,E., Chiang,Y.M., Wang,C.C. and Keller,N.P. (2013) VeA and MvlA repression of the cryptic orsellinic acid gene cluster in *aspergillusnidulans* involves histone 3 acetylation. *Mol. Microbiol.*, **89**, 963–974.
29. Chen,Y., Kistler,H.C. and Ma,Z.H. (2019) *Fusarium graminearum* trichothecene mycotoxins: biosynthesis, regulation, and management. *Annu. Rev. Phytopathol.*, **57**, 15–39.
30. McMullen,M., Jones,R. and Gallenberg,D. (1997) Scab of wheat and barley: a re-emerging disease of devastating impact. *Plant Dis.*, **81**, 1340–1348.
31. Gu,Q., Chen,Y., Liu,Y., Zhang,C. and Ma,Z.H. (2015) The transmembrane protein fgsho1 regulates fungal development and pathogenicity via the MAPK module ste50-ste11-ste7 in *fusariumgraminearum*. *New Phytol.*, **206**, 315–328.
32. Weitz,H.J., Ballard,A.L., Campbell,C.D. and Killham,K. (2001) The effect of culture conditions on the mycelial growth and luminescence of naturally bioluminescent fungi. *FEMS Microbiol. Lett.*, **202**, 165–170.
33. Yun,Y., Liu,Z., Zhang,J., Shim,W.B., Chen,Y. and Ma,Z. (2014) The MAPKK fgmkk1 of *fusariumgraminearum* regulates vegetative differentiation, multiple stress response, and virulence via the cell wall integrity and high-osmolarity glycerol signaling pathways. *Environ. Microbiol.*, **16**, 2023–2037.
34. Park,G., Bruno,K.S., Staiger,C.J., Talbot,N.J. and Xu,J.R. (2004) Independent genetic mechanisms mediate turgor generation and penetration peg formation during plant infection in the rice blast fungus. *Mol. Microbiol.*, **53**, 1695–1707.
35. Chen,A., Ju,Z., Wang,J., Wang,J., Wang,H., Wu,J., Yin,Y., Zhao,Y., Ma,Z.H. and Chen,Y. (2020) The RasGEF fgcdc25 regulates fungal development and virulence in *fusariumgraminearum* via cAMP and MAPK signalling pathways. *Environ. Microbiol.*, **22**, 5109–5124.
36. Jiang,C., Cao,S., Wang,Z., Xu,H., Liang,J., Liu,H., Wang,G., Ding,M., Wang,Q., Gong,C. *et al.* (2019). An expanded subfamily of G-protein-coupled receptor genes in *fusariumgraminearum* required for wheat infection. *Nat Microbiol*, **4**, 1582–1591.
37. Barbez,E., Dünser,K., Gaidora,A., Lendl,T. and Busch,W. (2017). Auxin steers root cell expansion via apoplastic pH regulation in *arabidopsisthaliana*. *Proc. Natl. Acad. Sci. U.S.A.*, **114**, e4884–e4893.
38. Dang,X., Chen,B., Liu,F., Ren,H., Liu,X., Zhou,J., Qin,Y. and Lin,D. (2020). Auxin signaling-mediated apoplastic pH modification functions in petal conical cell shaping. *Cell Rep.*, **30**, 3904–3916.
39. Sasaki,A., Yamaji,N., Xia,J. and Ma,J.F. (2011) OsYSL6 is involved in the detoxification of excess manganese in rice. *Plant Physiol.*, **157**, 1832–1840.
40. Shen,Q., Liang,M., Yang,F., Deng,Y.Z. and Naqvi,N.I. (2020) Ferroptosis contributes to developmental cell death in rice blast. *New Phytol.*, **227**, 1831–1846.
41. Chen,S., Zhou,Y., Chen,Y. and Gu,J. (2018) fastp: an ultra-fast all-in-one FASTQ preprocessor. *Bioinformatics*, **34**, i884–i890.
42. Kim,D., Paggi,J.M., Park,C., Bennett,C. and Salzberg,S.L. (2019) Graph-based genome alignment and genotyping with HISAT2 and HISAT-genotype. *Nat. Biotechnol.*, **37**, 907–915.
43. Pertea,M., Pertea,G.M., Antonescu,C.M., Chang,T.C., Mendell,J.T. and Salzberg,S.L. (2015) StringTie enables improved reconstruction of a transcriptome from RNA-seq reads. *Nat. Biotechnol.*, **33**, 290–295.
44. Love,M.I., Huber,W. and Anders,S. (2014) Moderated estimation of fold change and dispersion for RNA-seq data with DESeq2. *Genome Biol.*, **15**, 550.
45. Kaufmann,K., Muino,J.M., Osteras,M., Farinelli,L., Krajewski,P. and Angenent,G.C. (2010) Chromatin immunoprecipitation (ChIP)

of plant transcription factors followed by sequencing (ChIP-SEQ) or hybridization to whole genome arrays (ChIP-CHIP). *Nat. Protoc.*, **5**, 457–472.

46. Chen,Y., Chen,Y., Shi,C., Huang,Z., Zhang,Y., Li,S., Li,Y., Ye,J., Yu,C., Li,Z. *et al.* (2018) SOAPnuke: a mapreduce acceleration-supported software for integrated quality control and preprocessing of high-throughput sequencing data. *GigaScience*, **7**, 1–6.

47. Langmead,B. and Salzberg,S. (2012) Fast gapped-read alignment with bowtie 2. *Nat. Methods*, **9**, 357–359.

48. Ramirez,F., Dundar,F., Diehl,S., Gruning,B.A. and Manke,T. (2014) deepTools: a flexible platform for exploring deep-sequencing data. *Nucleic Acids Res.*, **42**, 187–191.

49. Robinson,J.T., Thorvaldsdóttir,H., Winckler,W., Guttman,M., Lander,E.S., Getz,G. and Mesirov,J.P.J.N.b. (2011) Integrative genomics viewer. *Nat. Biotechnol.*, **29**, 24–26.

50. Wienken,C.J., Baaske,P., Rothbauer,U., Braun,D. and Duhr,S. (2010) Protein-binding assays in biological liquids using microscale thermophoresis. *Nat. Commun.*, **1**, 100.

51. Zhao,M., Geng,R., Guo,X., Yuan,R., Zhou,X., Zhong,Y., Huo,Y., Zhou,M., Shen,Q., Li,Y. *et al.* (2017) PCAF/GCN5-mediated acetylation of RPA1 promotes nucleotide excision repair. *Cell Rep.*, **20**, 1997–2009.

52. Hellman,L.M. and Fried,M. (2007) Electrophoretic mobility shift assay (EMSA) for detecting protein-nucleic acid interactions. *Nat. Protoc.*, **2**, 1849–1861.

53. Masachis,S., Segorbe,D., Turra,D., Leon-Ruiz,M., Furst,U., El Ghalid,M., Leonard,G., Lopez-Berges,M.S., Richards,T.A., Felix,G. *et al.* (2016) A fungal pathogen secretes plant alkalinizing peptides to increase infection. *Nat Microbiol*, **1**, 16043.

54. Prusky,D., McEvoy,J.L., Leverentz,B. and Conway,W.S. (2001) Local modulation of host pH by *colletotrichum* species as a mechanism to increase virulence. *Mol Plant Microbe Interact*, **14**, 1105–1113.

55. Fernandes,T.R., Segorbe,D., Prusky,D. and Di Pietro,A. (2017) How alkalinization drives fungal pathogenicity. *PLoS Pathog.*, **13**, e1006621.

56. Greenshields,DL, Liu,G, Feng,J, Selvaraj,G. and Wei,Y. (2007) The siderophore biosynthetic gene SID1, but not the ferroxidase gene FET3, is required for full *fusariumgraminearum* virulence. *Mol. Plant Pathol.*, **8**, 411–421.

57. Park,Y.S, Kim,T.H, Chang,H.I, Sung,H.C. and Yun,C.W. (2006) Cellular iron utilization is regulated by putative siderophore transporter fgsit1 not by free iron transporter in *fusariumgraminearum*. *Biochem. Biophys. Res. Commun.*, **345**, 1634–1642.

58. Wang,Z.H., Ma,T.L., Huang,Y.Y., Wang,J., Chen,Y., Kistler,H.C., Ma,Z.H. and Yin,Y.N. (2019) A fungal ABC transporter fgatm1 regulates iron homeostasis via the transcription factor cascade fgarea-hapX. *PLoS Pathog.*, **15**, e1007791.

59. Schrettl,M., Kim,H.S., Eisendle,M., Kragl,C., Nierman,W.C., Heinekamp,T., Werner,E.R., Jacobsen,I., Illmer,P., Yi,H. *et al.* (2008) SreA-mediated iron regulation in *aspergillusfumigatus*. *Mol. Microbiol.*, **70**, 27–43.

60. Gsaller,F., Hortschansky,P., Beattie,S.R., Klammer,V., Tuppatsch,K., Lechner,B.E., Rietzschel,N., Werner,E.R., Vogan,A.A., Chung,D. *et al.* (2014) The janus transcription factor HapX controls fungal adaptation to both iron starvation and iron excess. *EMBO J.*, **33**, 2261–2276.

61. Oberegger,H., Schoeser,M., Zadra,I., Abt,B. and Haas,H. (2001) SREA is involved in regulation of siderophore biosynthesis, utilization and uptake in *aspergillusnidulans*. *Mol. Microbiol.*, **41**, 1077–1089.

62. Chung,K.R., Wu,P.C., Chen,Y.K. and Yago,J.I. (2020) The siderophore repressor SreA maintains growth, hydrogen peroxide resistance, and cell wall integrity in the phytopathogenic fungus *alternariaalternata*. *Fungal Genet. Biol.*, **139**, 103384.

63. Orejas,M., Espeso,E.A., Tilburn,J., Sarkar,S., Arst,H.N. Jr and Penalva,M.A. (1995) Activation of the *Aspergillus* PacC transcription factor in response to alkaline ambient pH requires proteolysis of the carboxy-terminal moiety. *Genes Dev.*, **9**, 1622–1632.

64. Hervas-Aguilar,A., Rodriguez,J.M., Tilburn,J., Arst,H.N. Jr and Penalva,M.A. (2007) Evidence for the direct involvement of the proteasome in the proteolytic processing of the *aspergillusnidulans* zinc finger transcription factor pacC. *J. Biol. Chem.*, **282**, 34735–34747.

65. Espeso,E.A., Tilburn,J., Sanchez-Pulido,L., Brown,C.V., Valencia,A., Arst,H.N. Jr and Penalva,M.A. (1997) Specific DNA recognition by the *Aspergillus nidulans* three zinc finger transcription factor pacC. *J. Mol. Biol.*, **274**, 466–480.

66. Fernandez-Martinez,J., Brown,C.V., Diez,E., Tilburn,J., Arst,H.N. Jr, Penalva,M.A. and Espeso,E.A. (2003) Overlap of nuclear localisation signal and specific DNA-binding residues within the zinc finger domain of pacC. *J. Mol. Biol.*, **334**, 667–684.

67. Wang,H.B., Dienemann,C., Stutzer,A., Urlaub,H., Cheung,A.C.M. and Cramer,P. (2020) Structure of the transcription coactivator SAGA. *Nature*, **577**, 717–720.

68. Setiaputra,D., Ross,J.D., Lu,S., Cheng,D.T., Dong,M.Q. and Yip,C.K. (2015) Conformational flexibility and subunit arrangement of the modular yeast spt-ada-gcn5 acetyltransferase complex. *J. Biol. Chem.*, **290**, 10057–10070.

69. Grant,P.A., Duggan,L., Cote,J., Roberts,S.M., Brownell,J.E., Candau,R., Ohba,R., Owen-Hughes,T., Allis,C.D., Winston,F. *et al.* (1997) Yeast gcn5 functions in two multisubunit complexes to acetylate nucleosomal histones: characterization of an ada complex and the SAGA (Spt/Ada) complex. *Gene Dev*, **11**, 1640–1650.

70. Laity,J.H., Lee,B.M. and Wright,P.E. (2001) Zinc finger proteins: new insights into structural and functional diversity. *Curr Opin Struc Biol*, **11**, 39–46.

71. Rossl,A., Denoncourt,A., Lin,M.S. and Downey,M. (2019) A synthetic non-histone substrate to study substrate targeting by the gcn5 HAT and sirtuin HDACs. *J. Biol. Chem.*, **294**, 6227–6239.

72. Whitmarsh,A.J. and Davis,R.J. (2000) Regulation of transcription factor function by phosphorylation. *Cell. Mol. Life Sci.*, **57**, 1172–1183.

73. Itoh,H., Matsuoka,M. and Steber,C.M. (2003) A role for the ubiquitin-26S-proteasome pathway in gibberellin signaling. *Trends Plant Sci.*, **8**, 492–497.

74. Geng,F., Wenzel,S. and Tansey,W.P. (2012) Ubiquitin and proteasomes in transcription. *Annu. Rev. Biochem.*, **81**, 177–201.

75. Chen,Y., Li,B., Xu,X., Zhang,Z. and Tian,S. (2018) The pH-responsive PacC transcription factor plays pivotal roles in virulence and patulin biosynthesis in *penicilliumexpansum*. *Environ. Microbiol.*, **20**, 4063–4078.

76. Niehaus,E.M., Janevska,S., von Bargen,K.W., Sieber,C.M., Harrer,H., Humpf,H.U. and Tudzynski,B. (2014) Apicidin F: characterization and genetic manipulation of a new secondary metabolite gene cluster in the rice pathogen *fusariumfujikuroi*. *PLoS One*, **9**, e103336.

77. Keller,N.P., Nesbitt,C., Sarr,B., Phillips,T.D. and Burow,G.B. (1997) pH regulation of sterigmatocystin and aflatoxin biosynthesis in *aspergillusspp*. *Phytopathology*, **87**, 643–648.

78. Trushina,N., Levin,M., Mukherjee,P.K. and Horwitz,B.A. (2013) PacC and pH-dependent transcriptome of the mycotrophic fungus *trichodermavirens*. *BMC Genomics*, **14**, 138.

79. Luo,Z., Ren,H., Mousa,J.J., Rangel,D.E., Zhang,Y., Bruner,S.D. and Keyhani,N.O. (2017) The PacC transcription factor regulates secondary metabolite production and stress response, but has only minor effects on virulence in the insect pathogenic fungus *Beauveria bassiana*. *Environ. Microbiol.*, **19**, 788–802.

80. Barda,O., Maor,U., Sadhasivam,S., Bi,Y., Zakin,V., Prusky,D. and Sionov,E. (2020) The pH-responsive transcription factor PacC governs pathogenicity and ochratoxin a biosynthesis in *Aspergillus carbonarius*. *Front. Microbiol.*, **11**, 210.

81. Wu,F.L., Zhang,G., Ren,A., Dang,Z.H., Shi,L., Jiang,A.L. and Zhao,M.W. (2016) The pH-responsive transcription factor PacC regulates mycelial growth, fruiting body development, and ganoderic acid biosynthesis in *Ganodermalucidum*. *Mycologia*, **108**, 1104–1113.

82. Yuan,L., Liu,X., Luo,M., Yang,S. and Wu,K. (2013) Involvement of histone modifications in plant abiotic stress responses. *J. Integr. Plant Biol.*, **55**, 892–901.

83. Shahbazian,M.D. and Grunstein,M. (2007) Functions of site-specific histone acetylation and deacetylation. *Annu. Rev. Biochem.*, **76**, 75–100.

84. Koutelou,E., Hirsch,C.L. and Dent,S.Y. (2010) Multiple faces of the SAGA complex. *Curr. Opin. Cell Biol.*, **22**, 374–382.

85. Wu,C.J., Liu,Z.Z., Wei,L., Zhou,J.X., Cai,X.W., Su,Y.N., Li,L., Chen,S. and He,X.J. (2021) Three functionally redundant plant-specific paralogs are core subunits of the SAGA histone acetyltransferase complex in *Arabidopsis*. *Mol Plant*, **14**, 1071–1087.

86. Jeon,J., Kwon,S. and Lee,Y.H. (2014) Histone acetylation in fungal pathogens of plants. *Plant Pathol J*, **30**, 1–9.

87. Kuo,M.H., vom Baur,E., Struhl,K. and Allis,C.D. (2000) Gcn4 activator targets gcn5 histone acetyltransferase to specific promoters independently of transcription. *Mol. Cell*, **6**, 1309–1320.

88. Krebs,J.E., Kuo,M.H., Allis,C.D. and Peterson,C.L. (1999) Cell cycle-regulated histone acetylation required for expression of the yeast HO gene. *Genes Dev.*, **13**, 1412–1421.

89. Xing,J.W., Wang,T.Y., Liu,Z.S., Xu,J.Q., Yao,Y.Y., Hu,Z.R., Peng,H.R., Xin,M.M., Yu,F.T., Zhou,D.X. *et al.* (2015) General control nonrespressed protein5-mediated histone acetylation of ferric reductase defective3 contributes to iron homeostasis in *Arabidopsis*. *Plant Physiol.*, **168**, 1309–1320.

90. Pasricha,S.R., Lim,P.J., Duarte,T.L., Casu,C., Oosterhuis,D., Mleczko-Sanecka,K., Suciu,M., Da Silva,A.R., Al-Hourani,K., Arezes,J. *et al.* (2017) Hepcidin is regulated by promoter-associated histone acetylation and HDAC3. *Nat Commun.*, **8**, 403.

91. Srivastav,M.K., Agarwal,N., Poonia,P. and Natarajan,K. (2021) Interplay between transcriptional regulators and the SAGA chromatin modifying complex fine-tune iron homeostasis. *J. Biol. Chem.*, **297**, 100727.

92. Kong,X., van Diepeningen,A.D., van der Lee,T.A.J., Waalwijk,C., Xu,J., Xu,J., Zhang,H., Chen,W. and Feng,J. (2018) The *Fusarium graminearum* histone acetyltransferases are important for morphogenesis, DON biosynthesis, and pathogenicity. *Front. Microbiol.*, **9**, 54.

93. Duan,W.J., Duan,W.J., Zhang,X.Q., Yang,T.Z., Dou,X.W., Chen,T.G., Li,S.J., Jiang,S.J., Huang,Y.J. and Yin,Q.Y. (2010) A novel role of ammonia in appressorium formation of *alternariaalternata* (Fries) keissler, a tobacco pathogenic fungus. *J. Plant Dis. Protect.*, **117**, 112–116.

94. Penalva,M.A., Tilburn,J., Bignell,E. and Arst,H.N. (2008) Ambient pH gene regulation in fungi: making connections. *Trends Microbiol.*, **16**, 291–300.

95. Ortoneda,M., Guarro,J., Madrid,M.P., Caracuel,Z., Roncero,M.I.G., Mayayo,E. and Pietro,A.D. (2004) *Fusarium oxysporum* as a multihost model for the genetic dissection of fungal virulence in plants and mammals. *Infect. Immun.*, **72**, 1760–1766.

96. Lambert,M., BlanchinRoland,S., LeLouedec,F., Lepingle,A. and Gaillardin,C. (1997) Genetic analysis of regulatory mutants affecting synthesis of extracellular proteinases in the yeast *yarrowialipolytica*: identification of a RIM101/pacC homolog. *Mol. Cell. Biol.*, **17**, 3966–3976.

97. Ost,K.S., O'Meara,T.R., Huda,N., Esher,S.K. and Alspaugh,J.A. (2015) The *cryptococcusneoformans* alkaline response pathway: identification of a novel rim pathway activator. *PLos Genet.*, **11**, e1005159.

98. Downey,M. (2021) Non-histone protein acetylation by the evolutionarily conserved GCN5 and PCAF acetyltransferases. *Biochim Biophys Acta Gene Regul. Mech.*, **1864**, 194608.

99. Li,B., Jiang,S., Yu,X., Cheng,C., Chen,S.X., Cheng,Y.B., Yuan,J.S., Jiang,D.H., He,P. and Shan,L.B. (2015) Phosphorylation of trihelix transcriptional repressor ASR3 by MAP kinase4 negatively regulates *Arabidopsis* immunity. *Plant Cell*, **27**, 839–856.

100. Kim,S.A., LaCroix,I.S., Gerber,S.A. and Guerinot,M.L. (2019) The iron deficiency response in *Arabidopsis thaliana* requires the phosphorylated transcription factor URI. *Proc. Natl. Acad. Sci. U.S.A.*, **116**, 24933–24942.

101. Gratz,R., Brumbarova,T., Ivanov,R., Trofimov,K., Tuennermann,L., Ochoa-Fernandez,R., Blomeier,T., Meiser,J., Weidtkamp-Peters,S., Zurbriggen,M.D. *et al.* (2020) Phospho-mutant activity assays provide evidence for alternative phospho-regulation pathways of the transcription factor FER-like iron deficency-induced transcription factor. *New Phytol.*, **225**, 250–267.

102. Martins,T.S., Costa,V. and Pereira,C. (2018) Signaling pathways governing iron homeostasis in budding yeast. *Mol. Microbiol.*, **109**, 422–432.